



Microwave-Assisted Drying: A Review of the State-of-the-Art

P. Rattanadecho & N. Makul

To cite this article: P. Rattanadecho & N. Makul (2016) Microwave-Assisted Drying: A Review of the State-of-the-Art, Drying Technology, 34:1, 1-38, DOI: [10.1080/07373937.2014.957764](https://doi.org/10.1080/07373937.2014.957764)

To link to this article: <http://dx.doi.org/10.1080/07373937.2014.957764>



Accepted author version posted online: 21 May 2015.



Submit your article to this journal [↗](#)



Article views: 163



View related articles [↗](#)



View Crossmark data [↗](#)



REVIEW ARTICLE

Microwave-Assisted Drying: A Review of the State-of-the-Art

P. Rattanadecho^a and N. Makul^b

^aCenter of Excellence in Electromagnetic Energy Utilization in Engineering (CEEE), Thammasat University (Rangsit Campus), Khlong Luang, Prathum Thani, Thailand; ^bDepartment of Building Technology, Faculty of Industrial Technology, Phranakhon Rajabhat University, Bangkok, Thailand

ABSTRACT

Offering advantages of energy-saving rapid drying rates, short processing times, deep penetration of the microwave energy, instantaneous and precise electronic control, and clean heating processes, microwave-assisted drying (MWD) has become a popular method that is currently used for many materials and processes. This article presents a systematic and comprehensive review of experimental and theoretical studies regarding the kinetic mechanisms of MWD. Factors affecting, methods for measuring, and applications of the dielectric property are discussed. From the experimental perspective, laboratory- and commercial-scale MWD systems are elaborated, including the equipment used and the stability, safety, and regulation of MWD systems. Theoretical investigations of thermal and nonthermal equilibrium models and moving-load computational models are discussed. Finally, some future trends in the research and development of MWD systems are suggested.

KEYWORDS

Experimental; microwave-assisted drying (MWD); modeling; thermal applications

Introduction

Microwaves are electromagnetic waves with radiofrequencies ranging from 300 MHz to 300 GHz (wavelengths from 1.0 mm to 1.0 m). According to the International Telecommunications Union, the electromagnetic frequency band for non-telecommunications (e.g., industrial, scientific, and medical) purposes ranges from 6.765 MHz to 246 GHz, as tabulated in Table 1. Most such systems are operated between 433.92 MHz and 40 GHz.^[1,2]

Microwave-assisted drying (MWD) is a complicated phenomenon resulting from microwave heating via liquid vaporization.^[3] MWD is a particularly efficient technique for thermal processes. It has been reported to be at least twice as effective as conventional drying methods for dielectric materials, including food,^[4–10] biological tissue,^[11] wood,^[12,13] ceramic,^[14–16] oil,^[17] and others. In principle, the mechanism and direction of heat transfer differ between conventional and microwave heating methods. In conventional heating, the material is heated by an external heat source (from outside the material to be heated), and the heat is transferred from the outside inward. In contrast, microwave heating is based on the rapid polarization and depolarization of charged groups as the material is subjected to a microwave field, resulting in simultaneous internal heat generation.

Microwave heating offers many advantages compared to conventional methods, including the following^[3,18–20]:

- Rapid heating rates and short processing times, which save energy
- Deep penetration of the microwave energy (e.g., in a dielectric material, a microwave system operating at 2.45 GHz can typically penetrate several centimeters), which allows heat to be generated efficiently without directly contacting the materials to be dried
- Instantaneous and precise electronic control
- Unique and fine internal structural development, which may improve many properties of the dried material
- Clean heating processes that do not generate secondary waste

Theoretically, MWD should be useful for materials that exhibit excellent dielectric properties. These materials should be able to absorb microwave energy and convert it into heat very efficiently. Recently, many investigations and practices have reported using microwave heating for numerous applications, such as the drying of paper, textiles, and leather. Other uses have included polymer cross-linking, accelerated vulcanization, and high-temperature casting. Food and related industries are likely the largest consumers of microwave power consumption, as microwave systems are useful for freeze-drying, thawing, cooking, etc. Use of microwave energy can lower the drying temperature for

CONTACT P. Rattanadecho ✉ ratphadu@engr.tu.ac.th ☎ Center of Excellence in Electromagnetic Energy Utilization in Engineering (CEEE), Thammasat University (Rangsit Campus), 99 Moo 18, Klong 1, Khlong Luang, Pathumthani 12120, Thailand.

Color versions of one or more of the figures in the article can be found online at www.tandfonline.com/ldrt.

© 2016 Taylor & Francis

Table 1. Electromagnetic frequency ranges for industrial, scientific, and medical non-telecommunications purposes.

Frequency range		Bandwidth		Availability region(s)
Value	Unit	Value	Unit	
6.765–6.795	MHz	30	kHz	Subject to local acceptance
13.553–13.567	MHz	14	kHz	Worldwide
26.957–27.283	MHz	326	kHz	Worldwide
40.660–40.700	MHz	40	kHz	Worldwide
433.050–434.790	MHz	1.74	MHz	Europe, Africa, Iraq, the former Soviet Union, and Mongolia
902.000–928.000	MHz	26	MHz	Americas, Greenland, and some of the eastern Pacific Islands only (with some exceptions)
2.400–2.500	GHz	100	MHz	Worldwide
5.725–5.875	GHz	150	MHz	Worldwide
24.000–24.250	GHz	250	MHz	Worldwide
61.000–61.500	GHz	500	MHz	Subject to local acceptance
122.000–123.000	GHz	1	GHz	Subject to local acceptance
244.000–246.000	GHz	2	GHz	Subject to local acceptance

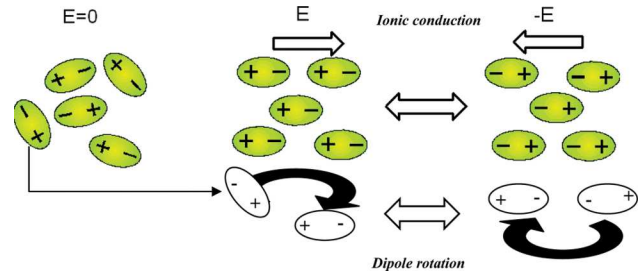
several dielectric materials, thereby reducing the incidence of drying imperfections, providing better throughput, increasing the energy efficiency, and reducing floor-space needs compared to conventional drying methods.

This article reviews experimental and theoretical studies of the kinetic mechanisms of MWD. Factors affecting methods for measuring and applications of the dielectric property are reviewed. From an experimental perspective, the equipment, stability, safety, and regulation of laboratory- and commercial-scale MWD systems are described in detail. Theoretical investigations of thermal and nonthermal equilibrium models and moving-load computational models are discussed. Finally, some future trends in the research and development of MWD are suggested.

Microwave heating mechanism

Microwave heating is directly associated with dielectric loss of the material. A material will absorb energy when placed in a high-frequency electric field. Consequently, electric dipole polarization and conduction will be generated within a dielectric material composed of polar molecules with positive and negative poles. These orderly dispersed polar molecules vibrate instantaneously and violently in response to the alternative high-frequency electric field of the microwave,^[18] as shown in Fig. 1. Resistance to molecular attraction and motion must be overcome. The temperature of the material increases as friction generates heat.

In mathematical terms, heat generation can be calculated from the root mean square of the electric field intensity, E . According to Lambert's law, the microwave

**Figure 1.** Mechanisms of microwave heating.^[18]

energy absorbed (or local volume of heat generated) can be defined as shown in Eq. (1)^[18]:

$$Q = \sigma |\vec{E}|^2 = 2\pi f \epsilon_0 \epsilon_r' (\tan \delta) |\vec{E}|^2 \quad (1)$$

where Q is the microwave energy, σ is the effective conductivity, f is the frequency (Hz), ϵ_0 is the permittivity of free space (8.8514×10^{-12} F/m), ϵ_r' is the relative dielectric constant, $\tan \delta$ is the loss tangent coefficient, and E is the electric-field intensity (V/m).

When microwave energy penetrates a dielectric material, the wave strength fades away exponentially because the microwave energy is absorbed by the dielectric material and converted into heat. This absorbed ratio varies with the frequency and dielectric property. In general, the penetration depth (D_p) is used to denote the depth of the power density. It decreases to 37% (or $1/e$) of its initial value at the surface^[18] and is defined in Eq. (2):

$$D_p = \frac{1}{\frac{2\pi f}{v} \sqrt{\epsilon_r' \left(\sqrt{1 + \left(\frac{\epsilon_r''}{\epsilon_r'} \right)^2} - 1 \right)}} = \frac{1}{\frac{2\pi f}{v} \sqrt{\frac{\epsilon_r' (\sqrt{1 + (\tan \delta)^2} - 1)}{2}}} \quad (2)$$

where D_p is the penetration depth, ϵ_r'' is the relative dielectric loss factor, and v is the microwave speed in the dielectric material, which can be evaluated by $c/\sqrt{\epsilon_r'}$.

From this equation, the penetration depth of a microwave depends on the dielectric property of the material. If the workpiece has very large dimensions and a high dielectric lossy factor, then its outer layer may overheat intermittently. In contrast, if the thickness of the workpiece is less than the penetration depth, then only a fraction of the microwave energy will be absorbed by the material.

Dielectric property

Theory underlying the dielectric property

As an intrinsic property that describes how a material interacts with the electric and magnetic fields of a

microwave, the dielectric property can be characterized by two independent properties: the complex electric permittivity, ϵ^* , and the complex magnetic permeability, μ^* . However, most common concrete materials are non-magnetic and yield a permeability μ^* that is very close to the permeability of free space ($4\pi \times 10^{-7} \text{ m} \cdot \text{kg} / \text{s}^2 \cdot \text{A}^2$).^[18] Thus, the complex electric permittivity, ϵ^* , which comprises real and imaginary parts, can be defined by the relationship in Eq. (3):

$$\epsilon_r^* = \epsilon_r' - j \epsilon_r'' \quad (3)$$

where ϵ_r' and ϵ_r'' are the real and imaginary parts, respectively, of the complex permittivity, and $j = \sqrt{-1}$. The dielectric constant ϵ_r' measures how much energy that is transferred from an external electric field is stored in a material. The relative loss factor ϵ_r'' measures how lossy a material is to an external electric field. The loss tangent $\tan \delta$, calculated as shown in Eq. (4), is an essential ratio of the energy lost (relative loss factor) to the energy stored (relative dielectric constant) in a material.

$$\tan \delta = \epsilon_r'' / \epsilon_r' \quad (4)$$

Factors affecting the dielectric properties of materials to be dried

The dielectric property of a material to be dried affects the microwave heating rate and energy consumption, as described in Eq. (1). The main factors that determine the dielectric behavior of dielectric materials include the frequency and temperature of microwave heating and the moisture content of the material. Llave et al.^[21] used the parallel-plate measurement method with an impedance analyzer and a dielectric test fixture to determine the dielectric properties of three ordinary tuna muscles at radiofrequencies of 13.56 and 27.12 MHz from -20 to $+10^\circ\text{C}$. Values of the dielectric constant (ϵ') were higher from -3 to 1°C than at other temperatures. Tuna samples with higher moisture contents exhibited higher values of the dielectric property than other samples, especially at lower frequencies.

The effects of moisture content on the dielectric constant and dielectric loss are well known. Regardless of the temperature, materials with higher moisture contents consistently exhibit higher values of the dielectric constant and dielectric loss, because the microwave absorption and dissipation increase with increasing free water in the material.^[2] However, there is no obvious relationship between temperature and the dielectric property. The ϵ' values increase lightly with increasing temperature at every moisture level. Nonetheless, a clear decrease in ϵ' values with increasing water content was found in some investigations.^[22–26] As well as the work

of Feng et al.,^[27] they indicated that the dielectric properties of food products that continually affect microwave drying characteristics are directly influenced by moisture content and temperature. This research also presented the contribution of different dispersion mechanisms in biological materials as affected by frequency and temperature, as shown in Fig. 2. Based on this investigation, it a strong moisture leveling effect was found when drying apples from 50% to 4% at elevated temperatures in 915 MHz or 2.45 GHz microwave drying systems. Further, moisture removal in dehydration operations resulted in a decrease in dielectric properties. Sipahioglu and Barringer^[28] found comparable behavior for garlic samples with 57.3% moisture content. S lyom et al.^[29] observed that when the temperature of milled seeds increased, the ϵ'' value gradually decreased, with a high amount of free water.

The dielectric constant (ϵ') and loss factor (ϵ'') of potato purees were observed to decrease considerably after freezing.^[32] From -25 to 5°C , the simultaneous addition of sucrose and salt increased the ϵ' and ϵ'' values of the samples, with salt having a greater influence than sucrose content on the dielectric properties. The addition of sucrose alone had an insignificant effect on the dielectric properties of thawing samples. In contrast, ϵ' decreased and ϵ'' increased with increasing salt content and temperature. In another study, Wang et al.^[33] considered the effects of blanching on the dielectric properties of potato purees. The dielectric loss and electrical conductivity values of microwave-blanching samples were two times higher than those of boiling water-blanching samples and five times higher than those of unblanching samples. For stem lettuce

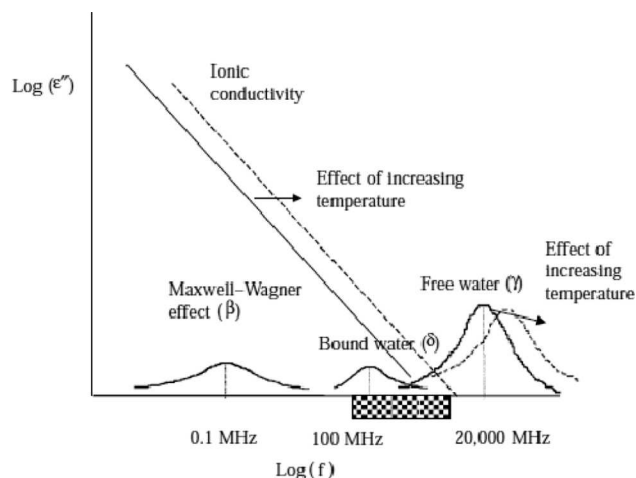


Figure 2. Contribution of different dispersion mechanisms in biological materials as affected by frequency and temperature^[30] based on Roebuck and Goldblith.^[2,31] The shaded range represents frequency range measured by Feng et al.^[27]

cubes, the values of these dielectric properties decreased considerably after freezing.

One method for creating a porous structure during fruit and vegetable drying is to use an instantaneous controlled pressure drop (DIC), which affects the dielectric properties of the food. Kristiawan et al.^[34] used DIC with an open-ended coaxial probe at a frequency of 915 MHz, in the temperature range of 20 to 90°C, with material having a wet bulk moisture content of 5–80%. The dielectric constant and loss factor values increased approximately linearly with increasing moisture content. When the products were treated by the DIC process (with moisture contents <20% wet bulk), the values of the dielectric constant and loss factor were slightly lower than the values of non-treated products.

Techniques for measuring the dielectric property

Many techniques have been developed to understand the dielectric property (Table 2), including the

transmission/reflection line, perturbation, free-space, and open-ended methods.^[35,36] Selection of the appropriate method depends, in part, on the operating frequency of the microwave system.^[36] For example, at the commonly utilized frequency of 2.45 ± 0.05 GHz, the dielectric property should be measured by transmission line. This method allows the measurement of specimens with a slab-shaped geometry to be placed across the cavity. However, this method is limited by the air-gap effect. The open-ended probe method could also be used, which involves measuring the phase and amplitude of the reflected signal at the end of an open-ended coaxial line inserted in a specimen. This method, too, has limitations due to the reflection effect from the specimen.

Choices of the measurement equipment and design of the sample holder depend on several factors, including the dielectric material to be characterized and the extent of the research, as well as the equipment and resources that are available. Two types of dielectric

Table 2. Summary of techniques for measuring the dielectric property.^[35,36]

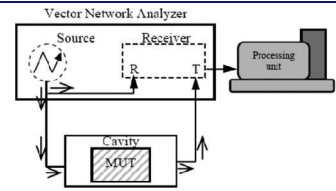
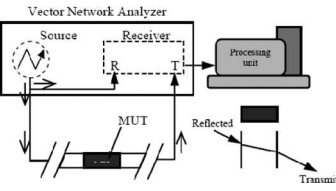
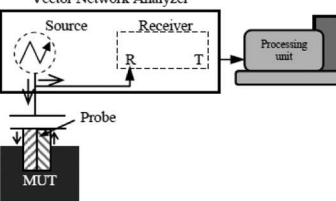
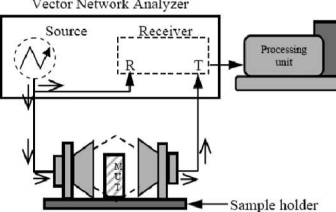
Technique	Characteristics	Feature	Dielectric properties
Perturbation (Cavity) (Resonant)	<p>The measurement is made by placing a sample completely through the center of a waveguide that has been made into a cavity.</p> <p>Advantages:</p> <ul style="list-style-type: none"> • simple and easy data reduction • accuracy and high temperature capability • suited to low dielectric loss materials <p>Disadvantages:</p> <ul style="list-style-type: none"> • need high frequency resolution vector network analysis (VNA) • limited to narrow band of frequency band only 		ϵ_r, μ_r
Transmission/reflection line	<p>The material under test (MUT) must be made into slab geometry.</p> <p>Advantages:</p> <ul style="list-style-type: none"> • common coaxial lines and waveguide • used to determine both ϵ_r, μ_r of the MUT <p>Disadvantages:</p> <ul style="list-style-type: none"> • limited by the air-gap effect • limited to low accuracy 		ϵ_r, μ_r
Open-ended probe	<p>The technique calculates the dielectric properties from the phase and amplitude of the reflected signal at the end of an open-ended coaxial line inserted into a sample to be measured.</p> <p>Advantages:</p> <ul style="list-style-type: none"> • after calibration, can be routinely measured in a short time <p>Disadvantages:</p> <ul style="list-style-type: none"> • available for reflection measurement 		ϵ_r
Free-space	<p>The sample is placed between a transmitting antenna and a receiving antenna, and the attenuation and phase shift of the signal are measured.</p> <p>Advantages:</p> <ul style="list-style-type: none"> • used for high frequency and allow non destructive measurement • measure MUT in hostile environment <p>Disadvantages:</p> <ul style="list-style-type: none"> • need large and flat MUT and diffraction effects at the edge of sample • limited to low accuracy 		ϵ_r, μ_r

Table 3. Test conditions for the C- and F-beds with a constant initial moisture content of 25% (dry basis).

Test condition	Magnetron power (W)	Magnetron position	Air temperature (°C)	Drying time (min)
Case 1	800 × 6	Side (1-10-2-11-3-12)	Ambient, 30	90
Case 2	800 × 6	Top (7-4-8-5-9-6)	Ambient, 30	80
Case 3	800 × 6	Top (7-4-8-5-9-6)	Hot air, 70	80

analyzers have recently been used: the scalar network analyzer and the vector network analyzer. Vector network analyzers are quite popular, very versatile, and useful for extensive studies; however, they are also very expensive. Although less expensive, scalar network analyzers and impedance analyzers are generally still too costly for many applications.

The HP 8510^[37] can measure the magnitude and phase characteristics of linear networks, such as filters, amplifiers, attenuators, and antennae. As with all network analyzers, the HP 8510 apparatus measures the reflection and transmission of electromagnetic waves at an interface. An incident signal generated by a radio frequency source is compared with the signal transmission through the analyzer or reflected from the wave input when passing through the waveguide. However, this method is strongly affected by the air-gap content, with high air content tending to decrease the dielectric property of the material. It is also influenced by the consistency of dielectric materials. In particular, when materials behave like liquids, the settling of the material under its own weight can result in the non-uniform behavior of the whole specimen. Consequently, the measurement results are not representative of the whole body of the specimen.

To perform the transmission/reflection-line technique, a sample is placed in a section of the waveguide or coaxial line, and the complex scattering parameters are measured at the two ports with a vector network analyzer. Note that the system must be calibrated before the measurements can be made. Both the reflected signal (S_{11}) and the transmitted signal (S_{21}) are measured. Various equations are used to relate the scattering parameters to the complex permittivity and permeability of the material. The S-parameters are converted to the complex dielectric parameters by solving the equations with the Nicholson-Ross-Weir (NRW) technique.^[37]

An open-probe technique can be applied to measure the dielectric properties of samples before MWD processing.^[14,38] For example, a portable dielectric network analyzer can be used over a frequency band from 1.5–2.6 GHz to measure the dielectric properties of wood, as shown in Fig. 3. A portable

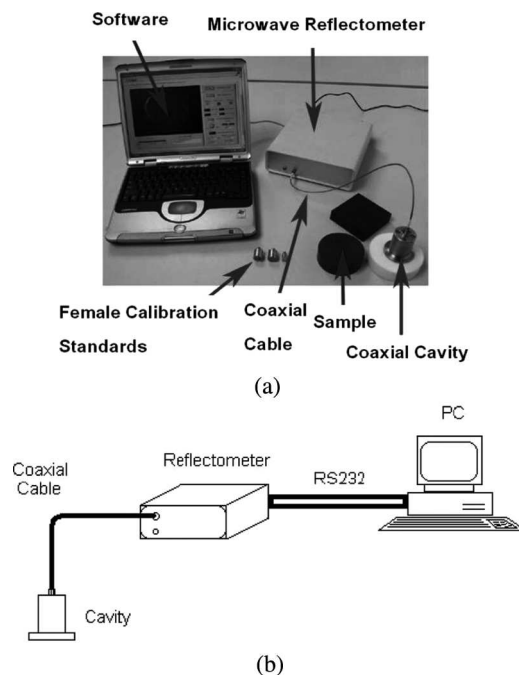


Figure 3. Portable dielectric network analyzer. Reprinted from Vongpradubchai and Rattanadecho^[14] with permission from Taylor & Francis.

dielectric measurement kit can be used to measure the complex permittivity values of a wide range of solid, semisolid, granular, and liquid materials. This system performs all of the necessary control functions, microwave signal treatments, calculations, and data-processing steps, and provides a representation of the results. The software controls the microwave reflectometer to measure the complex reflection coefficient of the tested material. It detects the cavity resonant frequency and quality factor, which it converts into the complex permittivity of the tested material. Finally, the measurement results are displayed in a graphical format or saved to disk.

Microwave systems

This section describes existing microwave systems, their components, and their functions, as well as various practical microwave systems based on the type of applicator. Conventionally, a microwave system should generate and introduce microwave energy to the (dielectric) material to be heated. A typical microwave system is shown in Fig. 4. Most microwave-heating systems consist of three basic components: a microwave power generator (usually a magnetron), waveguide, and microwave chamber/cavity where the specimen is processed. The system may also have supplementary components (e.g., control system, tuner, circulator, etc.).

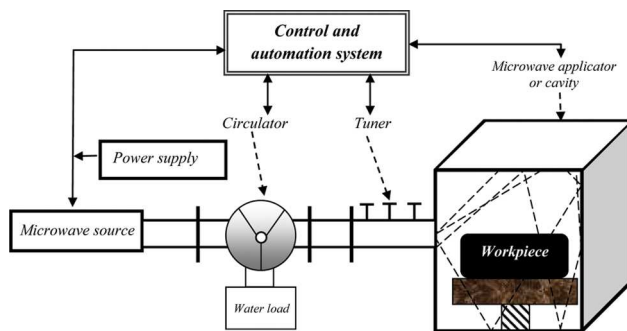


Figure 4. Schematic diagram of a typical microwave system.

As the most important component, the microwave power generator connects to the power supply unit and converts the alternating current of 50–60 Hz to

the desired high-frequency microwave radiation. This conversion is typically achieved by a magnetron, which must be shielded for safety and to prevent the leakage of harmonic radiation. The waveguide transmits microwave energy through free space and delivers it to the specimen. The waveguide is any structure that directs the propagation of energy in the form of an electromagnetic wave along a predetermined path.^[39] Waveguides may assume different physical forms, largely depending on the frequency band. Finally, the microwave chamber/cavity obeys electromagnetic laws, such that it can transmit, absorb, and reflect microwave energy.

Practically, microwave systems can be categorized according to the type of applicator that is associated

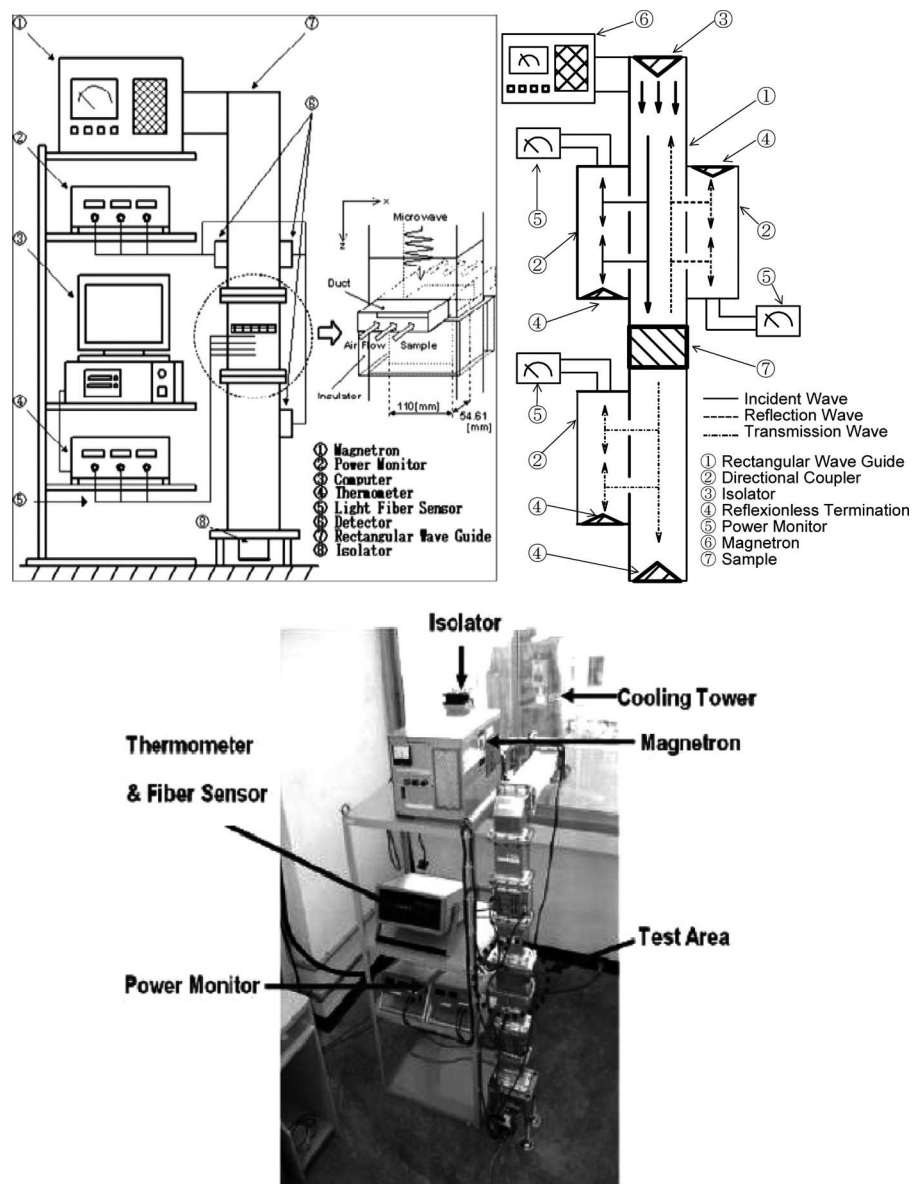
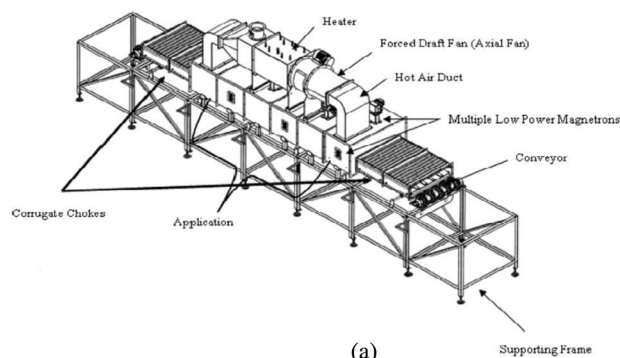
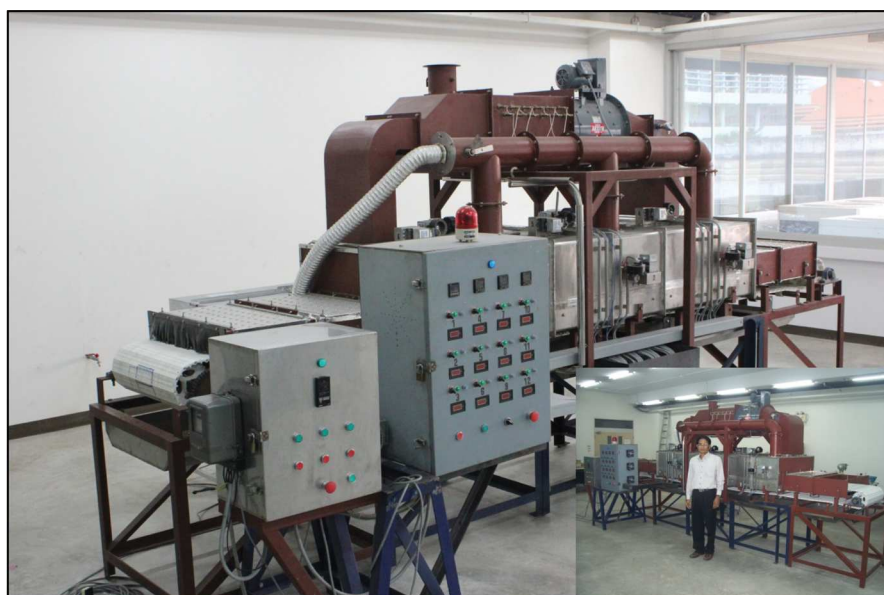
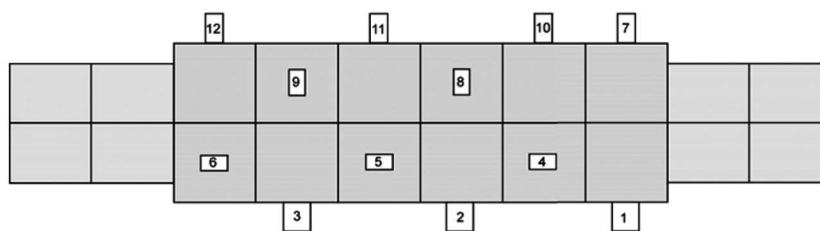


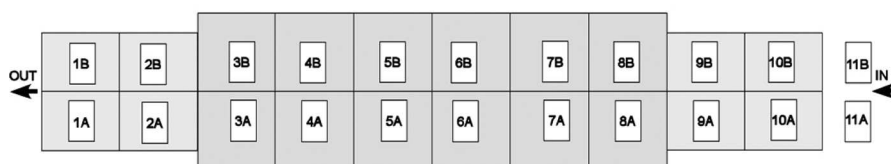
Figure 5. Example of a microwave system using a rectangular waveguide. Reprinted from Vongpradubchai and Rattanadecho^[14] with permission from Taylor & Francis.



(a)



(b)



(c)

Figure 6. (a) Combined multifeed microwave-convective air and continuous belt (CMCB) system. (b) Schematic diagram of the positioning of the 12 feed magnetrons and (c) 22 packed-bed feed samples. Reprinted from Jindarat et al.^[43] with permission from Taylor & Francis.

with the supplementary equipment or system, as follows:

- Traveling-wave applicator—A traveling wave is produced by matching the microwave source to a heated load, by using a rectangular or cylindrical waveguide.
- Near-field applicator—A resonant open-ended waveguide is used, or a cavity is attached directly to the end of a waveguide, and the energy is fed through slots into the cavity.
- Resonant applicators—These applicator types can be classified into single and multimode resonators, as

shown in Fig. 5 (single mode)^[14,40–42] and Fig. 6 (multimode).^[43,44]

- Single-mode resonant applicator: A standing wave applicator is attached to the end of a waveguide line that feeds power to the microwave. Magnetron-generated microwave energy is transmitted directly along the propagation direction (+z) of a rectangular waveguide toward a water load, situated at the end of the waveguide. This setup ensures that a minimal amount of microwave energy is reflected back to the sample. The warmed water load is circulated through a cooling tower.
- Multimode resonant applicator (Fig. 6a): Microwave power is generated by 12 compressed air-cooled magnetrons, which are installed in an asymmetric position around a rectangular microwave cavity (exterior dimensions: 900 × 450 × 2700 mm), as shown in Figs. 6b and 6c. Power is supplied directly to the drier by waveguides. The maximum microwave capacity is 9.6 kW at the operating frequency of 2.45 GHz, and the power setting can be adjusted in 800-W steps. The maximum working temperature is 180°C. Two open ends are essential in continuous processing equipment in order to allow the material to be heated to be placed on and removed from the conveyor belt. To maintain the microwave leakage $\leq 5 \text{ mW/cm}^2$ (as required by the U.S. Department of Health and Human Services), a mechanical blocking filter (corrugate choke) and microwave absorber zone filter are used at each of the open ends. To measure the specimen temperature, an infrared thermometer (accurate to $\pm 0.5^\circ\text{C}$) is installed at the opening ends after microwave processing. For example, a high-temperature microwave system generating microwave energy at 2.45 GHz and a maximum power of 6.0 kW with a multimode system can result in a sample temperature of 2000°C.

Experiments

Laboratory-scale

The goal of drying is to remove moisture from a material without causing any adverse effects on its chemical, physical, or related properties.^[45] MWD offers a high-performance drying method with multiple advantages, including fast drying rates and enhanced product quality, especially for food or other agricultural products. The microwave energy absorption level is strongly controlled by the initially wet product that can be used for determining heating of interior parts of material to be dried containing moisture and without distressing the exterior parts. MWD is well-characterized and very useful for the period in which the rate of drying is decreasing (also called the *falling rate period*). During this period, the diffusion is rate-limiting, leading to shrinkage of the whole structure and reduced moisture

content at the surface.^[46] Nevertheless, due to the occurrence of volumetric heating in MWD, gases are generated inside the material, while an internal pressure gradient develops that forces the water outside the material. As a result, MWD avoids the shrinkage of materials during drying. Furthermore, the combined use of MWD with other drying methods can improve the drying efficiency and product quality compared to using MWD or conventional drying alone.

However, especially during the final stages of MWD, excessive temperatures may develop along the corners or edges of the dried products, resulting in burning and byproduct production. It is difficult to control the final product temperature during hot-air MWD, and the product temperature should not exceed the hot-air temperature. For example, the penetration depth of microwave at an operating frequency of 2.45 GHz is inadequate for large-scale drying, whereas heating at 10–300 MHz can provide improved penetration depth. In special cases, fast mass transport might alter the product texture (e.g., cause “puffing” in food), which might be advantageous or disadvantageous depending on the required final product.^[46]

Incorporating a conventional drying method with MWD can enhance the drying rate, while maintaining the quality of the final product. In an important work, Feng and Tang^[47] evaluated a combined a spouted bed with microwave heating system to improve heating uniformity. A dryer was constructed for the drying tests. The system consisted of microwave source, rectangular cavity, hot-air source, spouted bed, and water load. In part of the spouted bed, it was constructed with microwave-transparent perspex which consisted of a cylindrical section and a 31° conical base as shown in Fig. 7. Based on the experimental investigation, drying

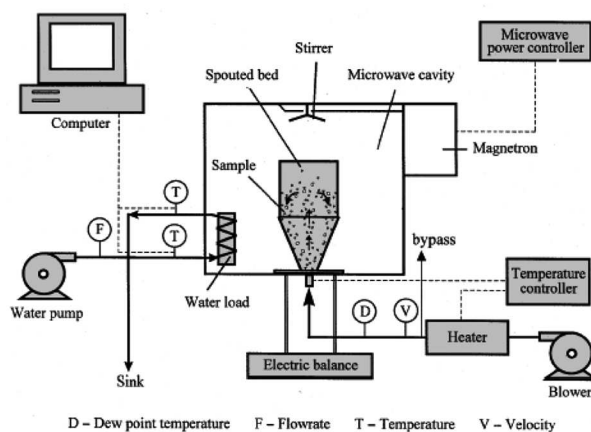


Figure 7. Schematic of microwave and spouted bed (MWSB) drying system. Reprinted from Feng and Tang^[47] with permission from Wiley.

tests were conducted at microwave power levels equivalent to 3.7, 4.9, and 6.1 W/g of evaporated apple dice. Evaporated Golden Delicious and Granny Smith apples were dried with a microwave power intensity of 4.9 W/g (wet basis). The hot air was controlled at 70°C. From this study, it can be found that the microwave and spouted bed (MWSB) method provided much more uniform heating within the microwave cavity. In addition, the drying time can be reduced moisture from evaporated apples to low moisture dehydrated apples (~5%) was significantly shortened as shown in Fig. 8.

Huang et al.^[48] compared the effects of conventional freeze drying (CFD), microwave freeze drying (MFD), microwave vacuum drying (MVD), and conventional vacuum drying (CVD) on the texture, color, rehydration, sensory characteristics, and microstructure of chips made by blending apples with potatoes. The equipment consisted of two drying cavities, as shown in Fig. 9. Experimental test results revealed that the quality of MFD chips was better than that of CFD chips, and MFD required about half the time as CFD to dry materials to the same moisture content. The rehydration rate of MFD chips was about the same as that of CFD products, while the water retention of MFD samples was higher.

Jiang et al.^[49] prepared banana chips through CFD and MFD methods in a dryer with a vacuum system, cold trap, and heating system. MFD decreased energy consumption by up to 35.7% and drying time by up to 40% compared to CFD. Increasing the heating power in the second drying stage of the MFD process decreased the energy consumption and drying time.

MVD has been widely considered as a high-performance dehydration method to achieve high-quality dried food products.^[50] Wang et al.^[51] studied the effects of gel type (i.e., cassava starch gel, fish gel,

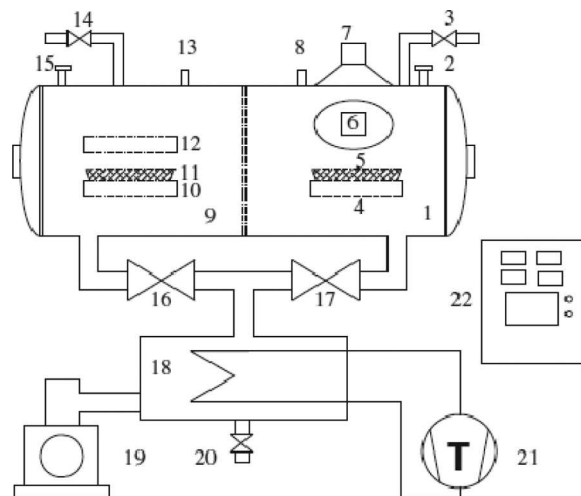


Figure 9. Schematic diagram of the microwave freeze dryer. 1, MFD chamber; 2, optical fiber temperature sensor; 3, MFD vacuum breakage valve; 4, sample supporting plate; 5, MFD sample; 6 and 7, microwave source; 8, pressure sensor for MFD chamber; 9, CFD chamber; 10 and 12, heating plate; 11, CFD sample; 13, pressure sensor for CFD chamber; 14, CFD vacuum breakage valve; 15, temperature sensor; 16, CFD vacuum valve; 17, MFD vacuum valve; 18, cold trap; 19, vacuum pump; 20, draining valve; 21, refrigeration compressor; and 22, control system. Reprinted from *Journal of Food Engineering*, Vol. 103, L. Huang, M. Zhang, A. S. Mujumdar, and R.-X. Lim, "Comparison of four drying methods for re-structured mixed potato with apple chips," pp. 279–284, 2011, with permission from Elsevier.

or mixed gel) and thermal treatment on the structure and quality of gel slices submitted to MVD. They used a lab-scale microwave-vacuum dryer in which the materials were rotated in the cavity, as described by Zhang et al.^[52] The microwave-vacuum dryer was operated at an absolute pressure of 5 kPa and a turntable rotation speed of 5 rpm. The power intensity for each drying test was 2.1 W/g of the original mass of sample. The gel type and preparation conditions had profound effects on the gel characteristics, influencing the structure and quality attributes of the MVD-derived products.

An essential aspect when using laboratory-scale MWD systems regards the prediction of the final quality of the dried product. Using Young's modulus as a measured parameter for texture, a framework for predicting the effective modulus of a solid food material was developed and extended to four moisture-removal processes: frying, drying, microwave heating, and baking. Moisture and temperature data required for predicting Young's modulus were obtained from multiphase porous media-based models of the processes. In this way, the process and product parameters could be used to make physics-based predictions of texture.^[53]

For the important effect on the drying, Namsangan et al.^[54] investigated an innovative two-stage drying concept. The work studied drying of shrimp using

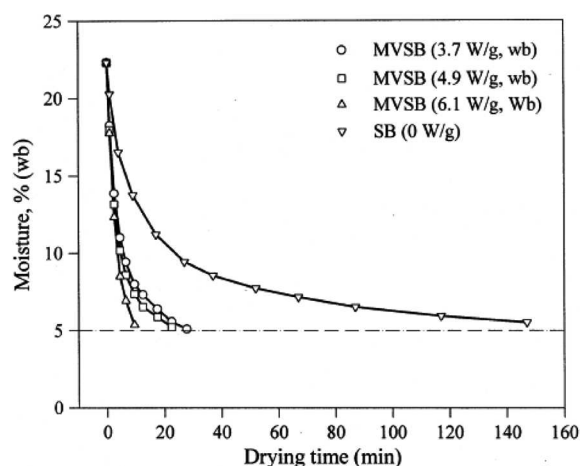


Figure 8. Drying curves of Red Delicious apples dried with MWSB method with different microwave power levels. Reprinted from Feng and Tang^[47] with permission from Wiley.

a superheated steam dryer. Shrinkage, color, rehydration behavior, toughness and hardness, and microstructure of dried shrimp were measured. The results indicated that a superheated steam dryer followed by a hot air dryer can offer redder shrimp compared to shrimp dried in a single-stage superheated steam dryer and no improvement in terms of shrinkage and rehydration behavior.

Commercial-scale

Hybrid systems associated with supplementary systems

Using a hybrid microwave system associated with supplementary systems can considerably enhance the drying rate and the final product quality. Jindarat et al.^[43] constructed a combined multifeed microwaved-convective air and continuous belt (CMCB) system, as shown in Fig. 6. They analyzed the energy consumption during drying of a non-hygroscopic porous packed bed, focusing on conditions of industrialized microwave processing. The overall drying and energy consumption results depended on the porosity of structure, hot-air temperature, and magnetron location. Using continuous microwave application had several advantages over the conventional method, such as shorter processing times, volumetric dissipation of energy throughout the product, and less energy consumption. Their results provide a fundamental understanding of the drying process using an industrial-size CMCB system.

Recently, Charoenvai et al.^[55] compared a single microwave dryer with a combination microwave-hot-air dryer in terms of their product properties and energy consumption during the drying of Durian peel particle boards. Their results showed that a CMBM would consume less energy than the single-microwave system (specific energy consumption (SEC) of 0.16509 MJ/kg), while providing the same or better product qualities than the combined system. These findings indicate the potential of the CMCB system to reduce electrical energy consumption. Moreover, using the combined system permitted quicker drying at an increased hot-air temperature. If this CMBM technology were to be implemented in industry, it could decrease production costs by lowering electrical energy consumption microwave-hot-air dryer in terms of their product properties and energy consumption during the drying of Durian peel particle boards. Their results showed that a CMBM would consume less energy than the single-microwave system (SEC of 0.16509 MJ/kg), while providing the same or better product qualities than the combined system. These findings indicate the potential of the CMCB system to reduce electrical energy consumption.

Moreover, using the combined system permitted quicker drying at an increased hot-air temperature. If this CMBM technology were to be implemented in industry, it could decrease production costs by lowering electrical energy consumption.

In 2013, Jindarat et al.^[56] analyzed the energy consumption during the drying of biomaterials using a combined unsymmetrical double-feed microwave and vacuum system (CUMV). The CUMV drying was more rapid in the continuous than in the pulsed microwave operation mode. Figures 10a and 10b show the rough color shades of tea leaves dried by the pulsed and continuous microwave operation modes, respectively. The best color was achieved by continuous MWD. Furthermore, the specific energy consumption values were relatively low in the continuous compared to the pulsed microwave operation mode.

The industrial-hybrid microwave system has been developed continuously by many microwave manufacturers such as Püschner and his group,^[57] such as a microwave freeze drying, which can cut down drying time from days into hours, as well as Micro Denshi,^[58] who constructs the microwave continuous equipment. It can be used to drying of equipment of ceramic molding, ferrite products swelling, and equipment for snack foods.

Safety and regulation

The health and safety of microwave processing cannot be neglected when microwave systems are operated by humans or in an environment where humans are present. This section details the limitations and conditions of microwave exposure, as regulated by relevant associations. Microwave processing of dielectric materials may involve a risk of microwave exposure to humans and biological tissues if certain precautions are not taken into account. The U.S. Federal Communication



Figure 10. Tea leaves dried under vacuum pressure at 385 Torr, with the (a) pulsed or (b) continuous microwave operation mode at a microwave power of 800 W. Reprinted from Jindarat et al.^[56] with permission from Taylor & Francis.

Commission and Occupational Health and Safety Administration^[59] have provided exposure limits for microwave energy, considering the effects of microwave radiation on human health from the perspectives of exposure source (e.g., medical devices, amateur radio, cellular phone base stations, hand-held cell phones, heating and sealing devices, microwave ovens, radio broadcast antennae, traffic radar devices, etc.), hazard location, exposure time, and solution. Absorption and distribution of microwave energy are strongly dependent on body size and orientation, as well as the frequency and polarization of the incident radiation.

The specific absorption rate refers to the power absorbed by a body when exposed to electromagnetic radiation. The current specific absorption rate limit is 4 W/kg. To be conservative, organizations generally use 1/10th of this value for setting standards, especially for radiofrequency and microwave exposure limits. For occupational exposure, the field strength is averaged over a 6-min time period. For public exposure, the field strength is averaged over a 30-min period, as recommended by guidelines or standards of the International Radiation Protection Association,^[60] the Institute of Electrical and Electronics Engineers,^[61,62] the National Radiological Protection Board, and the Health Protection Agency.^[63] It is strongly recommended that laboratory and industrial microwave systems be tested periodically for any leakage, and that suitable measures be taken to stop any substantial leakage before the system is used further.

In the past, there have been reports on the effects of electromagnetic (EM) fields on the eye.^[64,65] Nevertheless, the analysis generally was conducted based on the maximum SAR values permitted by public safety standards.^[66,67] The research on transport phenomena in a porous medium subject to EM fields is sparse except for our group. Some researchers investigated the effects of EM fields on the eye temperature.^[68] However, most previous studies of human exposed to EM fields hardly considered the heat transfer causing an incomplete analysis to the results. The thermal modeling of human tissue is important as a tool to investigate the effect of external heat sources and to predict the abnormalities in the tissue. At the beginning, most studies of heat transfer analysis in the eye used a heat conduction equation.^[69–71] Some studies carried out on the natural convection in the eye based on heat conduction model.^[72,73] Ooi and Ng^[73,74] studied the effect of aqueous humor (AH) hydrodynamics on the heat transfer in the eye based on heat conduction model. Meanwhile, the bioheat equation, introduced by Pennes,^[75] which is based on the heat diffusion equation for a blood perfused tissue, is used for modeling of the heat

transfer in the eye as well.^[76,77] Ooi and Ng also developed a three-dimensional model of the eye,^[78] extending their 2-D model.^[78] Most previous studies of humans exposed to EM fields hardly considered the heat transfer, causing an incomplete analysis to the results. Therefore, modeling of heat transport in human tissue is needed to cooperate with the modeling of electromagnetic (EM) in order to completely explain their interaction characteristics for approaching such phenomena. In 2011, Wessapan et al.^[79] proposed a numerical study to simulate the effects of dielectric shield on the specific absorption rate (SAR) and the temperature increase in the human body exposed to leakage microwave energy. Figures 11a and 11b show a vertical cross-section through the middle plane of the human trunk model. The meshes of the human model as well as the SAR and temperature distribution in the case of unshielded human model exposed to the microwave power density of 5 mW/cm² at the frequency of 300 MHz. It is found that the temperature distributions are not proportional to the local SAR value, as shown in Fig. 11b.

In 2013, Wessapan and Rattanadech^[80] presented a numerical analysis of the SAR and the heat transfer in a heterogeneous human eye model exposed to EM fields of 900 and 1800 MHz. The SAR value and the temperature distribution in various tissues in the eye during exposure to EM fields were obtained by numerical simulation of EM wave propagation, and a heat transfer model was then developed based on the natural convection and porous media theories. EM energy is emitted by an EM radiation device and falls on the eye with a particular power density, as shown in Fig. 12a. Fig. 12b shows the simulation of an electric field pattern inside the eye exposed to the EM fields in TM mode operating at the frequencies of 900 and 1800 MHz propagating along the vertical cross-section human eye model. Due to the different dielectric characteristics of the various tissue layers at different operating frequencies, a different fraction of the supplied EM energy will become absorbed in each layer in the eye. In the next year, Wessapan and Rattanadech^[81] also published the influence of ambient temperature on heat transfer in the human eye during exposure to electromagnetic fields at 900 MHz. This work focused on the transport phenomena that occur within the eye exposed to EM fields in hot, moderate, and cold ambient temperatures. In this study, the effect of thermoregulation mechanisms has been neglected due to the small temperature increase occurred during exposure process. The convective coefficient due to the blood flow inside the sclera is set to 65 W/m²K.^[81] In order to study the heat transfer in the eye, the coupled model of EM wave propagation

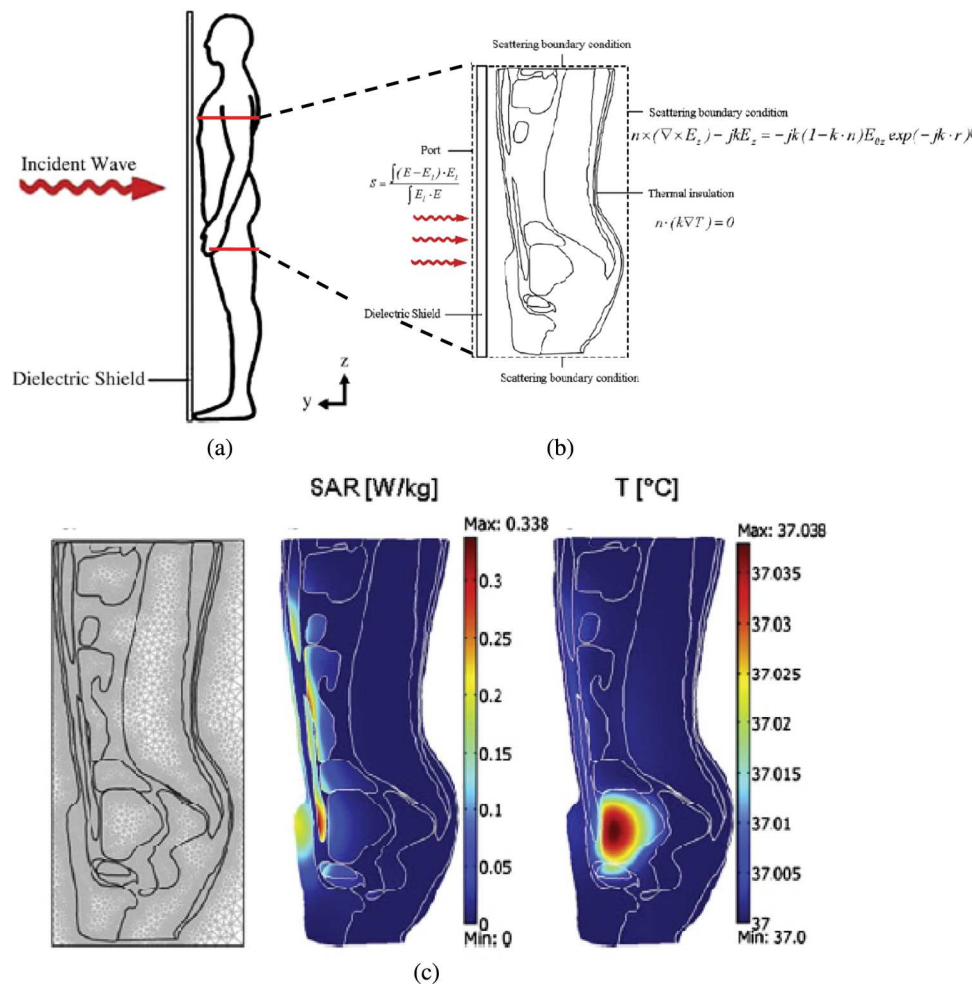


Figure 11. (a) Human model with dielectric shield. (b) Physical model and boundary condition used for analysis. (c) SAR and temperature distribution in the human model exposed to the microwave power density of 5 mW/cm^2 at the frequency of 300 MHz. Reprinted from *International Communications in Heat and Mass Transfer*, Vol. 38, T. Wessapan, S. Srisawatthisukul, and P. Rattanadecho, "The effects of dielectric shield on specific absorption rate and heat transfer in the human body exposed to leakage microwave energy," pp. 255–262, 2011, with permission from Elsevier.

and unsteady heat transfer as well as the boundary conditions is then investigated. Due to these coupled effects, the electric field distribution in Fig. 13 and the SAR distribution as shown in Fig. 14 are then converted into heat by absorption of the tissue.

Theoretical investigations

In theoretical analysis, the absorbed microwave power is generally assumed to decay exponentially into the absorbed material, as in Lambert's law. Although this law is valid for samples of large dimensions (in which the sample thickness is much larger than the penetration depth), it is not valid for small samples (in which the sample thickness is smaller than the penetration depth).^[82] The electromagnetic field within a small sample can be analyzed by solving Maxwell's equations. Two-dimensional (2D) models involving

Maxwell's equations have been used in the study of numerous heating processes in microwave applicator configurations.^[9,13] Most previous investigations considered simulations of microwave heating of homogeneous materials. Heat and mass transfer processes in porous materials have been studied from a theoretical perspective for several decades. To explain the physical phenomenon of drying in porous materials, most proposed theories use Whitaker's theory^[83] as a basis and take one of three approaches:

1. One-variable models employ a single diffusion equation and are used for simple configurations.
2. Two-variable models use two independent variables (temperature and moisture content) and neglect the effects of pressure buildup. These models can be used to describe the most important features of low-temperature drying.
3. Three-variable models use three independent variables (temperature, moisture content, and pressure

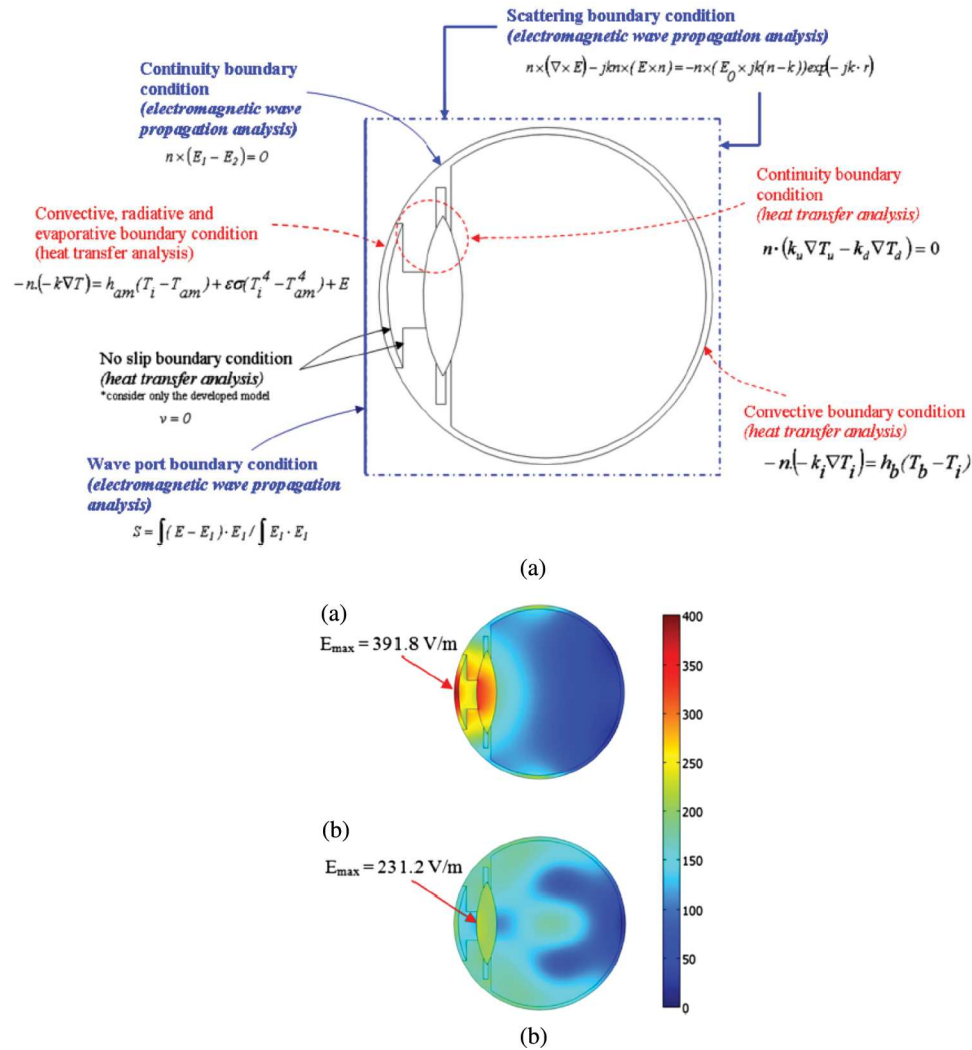


Figure 12. (a) EM wave propagation and heat transfer with boundary conditions and (b) electric field distribution (V/m) in human eye exposed to the EM power density of 100 mW/cm^2 at the frequencies of (a) 900 MHz and (b) 1800 MHz. Reprinted from *International Journal of Heat and Mass Transfer*, Vol. 64, T. Wessapan and P. Rattanadecho, "Specific absorption rate and temperature increase in the human eye due to electromagnetic fields exposure at different frequencies," pp. 426–435, 2013, with permission from Elsevier.

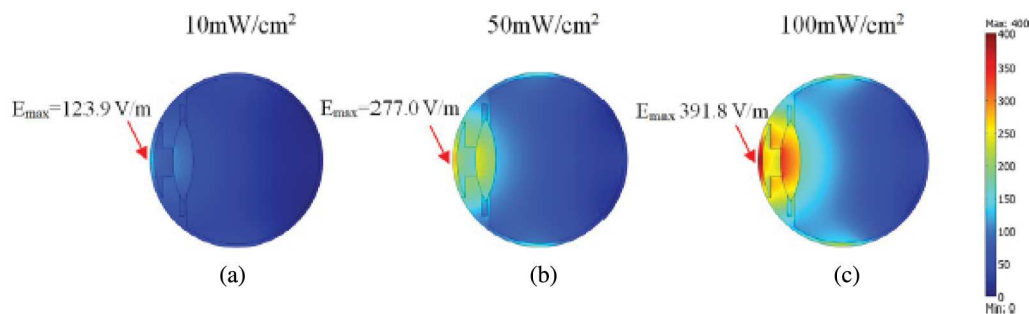


Figure 13. Electric field distribution (V/m) in the eye exposed to the EM power densities of (a) 10 mW/cm^2 , (b) 50 mW/cm^2 , and (c) 100 mW/cm^2 . Reprinted from *International Journal of Heat and Mass Transfer*, Vol. 70, T. Wessapan and P. Rattanadecho, "Influence of ambient temperature on heat transfer in the human eye during exposure to electromagnetic fields at 900 MHz," pp. 378–388, 2014, with permission from Elsevier.

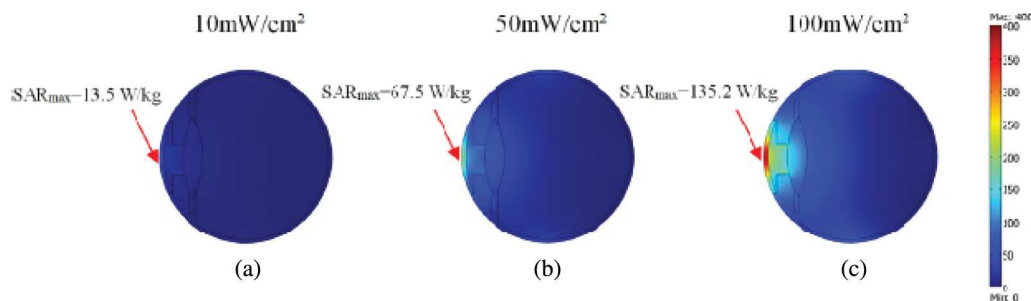


Figure 14. SAR distribution (W/kg) in the eye exposed to the EM power densities of (a) 10 mW/cm², (b) 50 mW/cm², and (c) 100 mW/cm². Reprinted from *International Journal of Heat and Mass Transfer*, Vol. 70, T. Wessapan and P. Rattanadecho, "Influence of ambient temperature on heat transfer in the human eye during exposure to electromagnetic fields at 900 MHz," pp. 378–388, 2014, with permission from Elsevier.

buildup), thereby providing more detail than two-variable models by describing all of the drying behaviors. Three-variable models can be used in cases of high-temperature convective drying, radio-frequency drying, etc.

Most studies have utilized one- or two-variable models in the case of conventional drying processes,^[84,85] because these models are easier to discretize and solve than three-variable models. A few studies have used three-variable models—notably, Perre and Turner,^[13] Ni and Datta,^[86] Feng et al.,^[87] and Rattanadecho et al.^[88] Some researchers have studied the interactions between microwave energy and heat and mass transfer phenomena of porous material, such as the microwave heating and drying processes.^[13,40,89] Most previous works have not mentioned 2-D pressure buildup or the flow field inside porous materials with varying particle sizes. A recent work performed a systematic investigation of heat and mass transport and pressure buildup phenomena during the MWD of a uniform porous packed bed under microwave energy at a frequency of 2.45 GHz using a rectangular waveguide (TE₁₀ mode).^[18] The unsaturated porous packed beds were composed by glass beads, water, and air. In this study, the effect of pressure buildup was neglected in the mathematical modeling. It was found that the particle size and thickness of the porous packed bed were primary factors determining heat and mass transport with multiphase flow.

Thermal equilibrium model for drying

Studying microwave-assisted batch fluidized bed drying, Chen et al.^[90] examined three microwave heating patterns (uniform, sinusoidal, and rectangular) with a constant average electric field strength of 1000 V/m. An apple was used as a representative porous material. Sinusoidal and rectangular heating patterns gave higher drying rates and shorter drying times than the uniform pattern under the same electric field strength. The

microwave power absorbed by particles varied with the electrical field strength during drying, and the average value gradually decreased with time. Intermittent microwave heating gave the shortest drying time but consumed the greatest amount of microwave energy.

Another important issue in microwave drying comes from microwave heating process regards hot-spot formation. Bhattacharya and Basak^[91] analyzed the temperature dynamics during microwave processing of 2% agar gel, potato, beef, and marinated shrimp. They assessed the role of the absorbed power in forecasting heating scenarios during microwave processing. They assumed uniform plane microwave radiations with incident intensities of I_L and I_R from the left and right sides, respectively, as shown in Fig. 15. The absorbed power distribution showed three distinct behavior regimes (i.e., thin, resonating, and thick sample), depending on the sample length and dielectric property of the material. Nearly uniform power distributions were

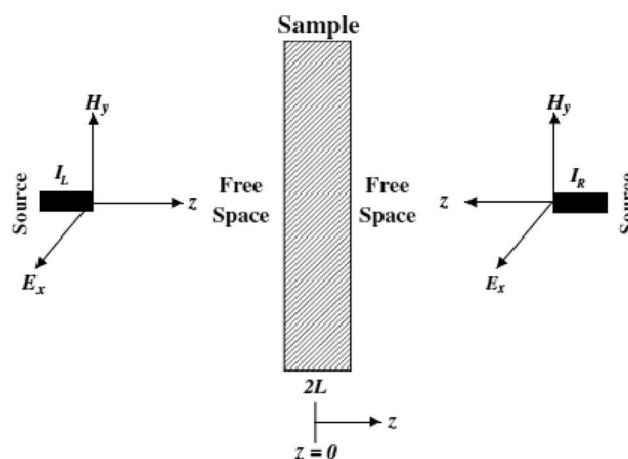


Figure 15. Schematic illustration of a 1-D sample exposed to plane electromagnetic radiations from the left and right sides. Reprinted from *Food Research International*, Vol. 39, M. Bhattacharya and T. Basak, "On the analysis of microwave power and heating characteristics for food processing: Asymptotes and resonances," pp. 1046–1057, 2006, with permission from Elsevier.

attained within thin samples, compared to exponential distributions within thick samples. In the resonating regime (between the thin and thick sample regimes), power distributions exhibited spatial oscillations.

To develop theoretical and experimental analyses of the MWD of uniform porous materials, Feng et al.^[87] developed a mathematical model to predict heat and mass transport in microwave and spouted bed combined (MWSB) drying of porous materials (diced apple). A total gas-pressure equation was taken into account internal vapor generation during microwave drying. The assumptions in the model are as follows: (a) local thermodynamic equilibrium exists. That is the solid, liquid, and gas phases at the same average temperature at any moment in the control volume; (b) solid, liquid, and gas phases are continuous; (c) binary gas mixture of air and vapor obeys the ideal gas; (d) local vapor pressure as a function of moisture content and temperature can be calculated sorption isotherm; and (e) the material used in this model is diced apple. In the model, transport relations as fluid velocity in a multiphase porous medium are given by the generalized Darcy's law. For governing equations considered in this study, mass transfer to occur only in the radial direction and one-dimensional problem in spherical coordinate was formulated. The total moisture transport equation can be written as

$$\frac{\partial X_l}{\partial t} = \frac{1}{r^2} \frac{\partial}{\partial r} \left[D_x r^2 \frac{\partial X_l}{\partial r} + D_T r^2 \frac{\partial T}{\partial r} + D_p r^2 \frac{\partial P_g}{\partial r} \right] \quad (5)$$

where $X_l \approx X_f + X_b$

$$D_X = D_X^f + D_X^b + D_X^v$$

$$D_T = D_T^f + D_T^b + D_T^v$$

$$D_P = D_P^f + D_P^b + D_P^v$$

A MWSB dryer was developed for drying test and validating the model simulation, as shown in Fig. 16. This system consisted of a 2.45 GHz microwave supply system and supply system. In this study, the constructed model can be used as an effective toll to predict moisture, temperature, and pressure for MWSB of the materials to be dried. For example, the case of moisture content for MWSB [microwave power = 4 W/g, air temperature = 70 °C, and SB (air temperature = 70 °C)] drying as shown in Fig. 17. It was found that simulation prediction is in good agreement with experiments for both drying methods.

In another investigation, Suwannapum and Rattanadecho^[92] numerically ascertained based on a one dimensional (1-D), three-variable method by studying the effects of sample thickness and size on the overall heat and multiphase flow, and then compared their

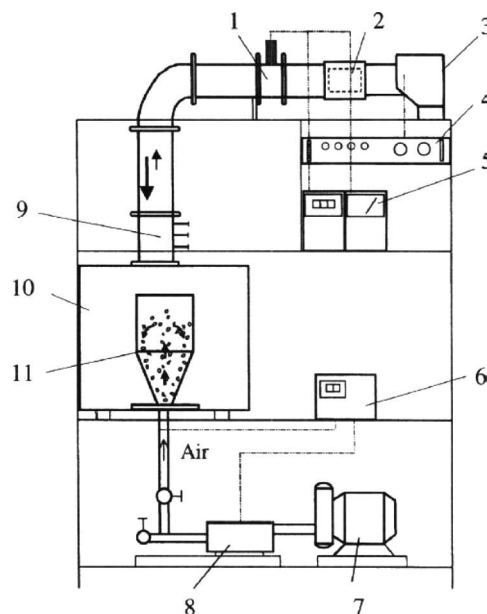


Figure 16. 2.45 GHz MWSB dryer. 1, Direction coupler; 2, circulation; 3, magnetron; 4, power controller; 5, power meter; 6, temperature controller; 7, air pump; 8, heater; 9, three-stub tuner; 10, Microwave cavity; 11, spouted bed. Reprinted from Feng et al.^[87] with permission from Wiley.

theoretical findings with experimental results. A schematic of the porous packed bed model used in the heat and mass transport analysis is shown in Fig. 18. Based on the conservation of mass and energy in capillary porous materials, the governing equation of mass and energy of all phases can be derived by the volume-averaging technique.^[83] From the results, it can be concluded that the particle size significantly affects the pressure buildup, water saturation, and fluid movement inside the unsaturated porous packed bed. In addition, the saturated distribution can change the electromagnetic field and heat and mass transfer patterns. The sample

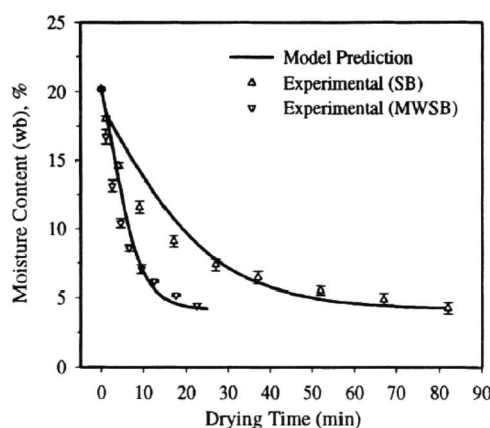


Figure 17. Moisture content: model prediction versus experimental results for MWSB (microwave power = 4 W/g, air temperature = 70 °C, and SB (air temperature = 70 °C) drying. Reprinted from Feng et al.^[87] with permission from Wiley.

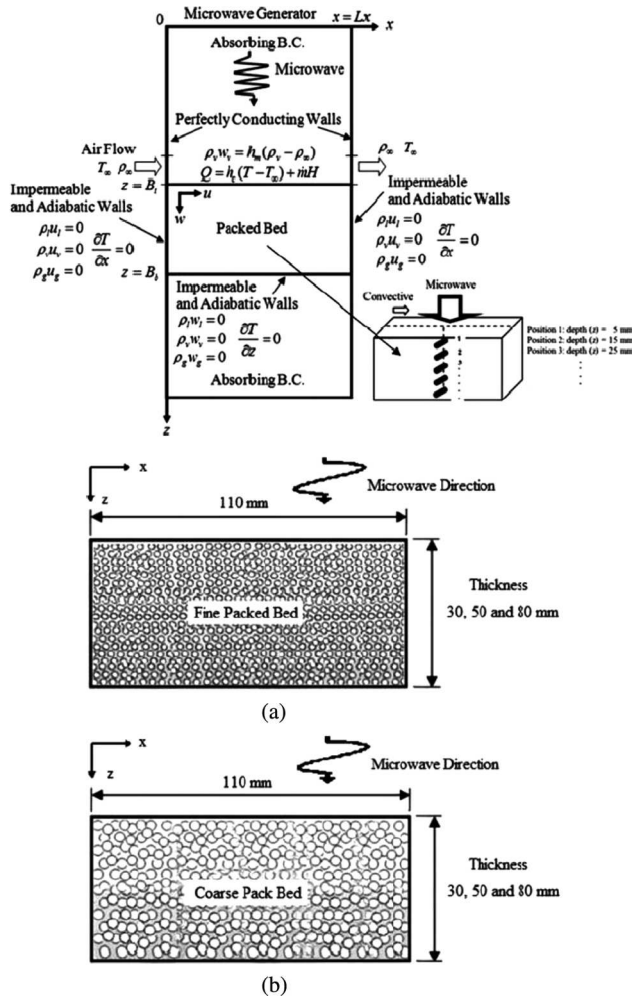


Figure 18. Physical model and measurement points. Reprinted from Suwannapum and Rattanadecho^[92] with permission from Taylor & Francis.

thickness strongly influenced heating behavior by changing the electromagnetic field patterns, microwave power absorption, and temperature distribution profile results.

By assuming that moisture transport in a sample can be described by the mass balance equations of water and water vapor, and considering Darcy's and Fick's laws, the moisture transport equation can be expressed in the 2D scalar form, as follows:

$$\begin{aligned} \phi \frac{\partial}{\partial t} \{ \rho_l s + \rho_v (1-s) \} + \frac{\partial}{\partial x} \left[\rho_l \frac{KK_{rl}}{\mu_l} \left(\frac{\partial p_c}{\partial x} - \frac{\partial p_g}{\partial x} \right) \right. \\ \left. + \rho_v \frac{KK_{rg}}{\mu_g} \left(-\frac{\partial p_g}{\partial x} \right) - D_m \frac{\partial p_y}{\partial x} \right] \\ + \frac{\partial}{\partial z} \left[\rho_l \frac{KK_{rl}}{\mu_l} \left(\frac{\partial p_c}{\partial z} - \frac{\partial p_g}{\partial z} + \rho_l g_z \right) \right. \\ \left. + \rho_v \frac{KK_{rg}}{\mu_g} \left(-\frac{\partial p_g}{\partial z} + \rho_l g_z \right) - D_m \frac{\partial p_y}{\partial z} \right] = 0 \end{aligned} \quad (6)$$

Again, considering Darcy's and Fick's laws and assuming that the gaseous phase is an ideal mixture of perfect gases, the pressure equation can be expressed in the 2D scalar form:

$$\begin{aligned} \phi \frac{\partial}{\partial t} \{ \rho_a (1-s) \} + \frac{\partial}{\partial x} \left[\rho_a \frac{KK_{rg}}{\mu_g} \left(-\frac{\partial p_g}{\partial x} \right) - D_m \frac{\partial p_a}{\partial x} \right] \\ + \frac{\partial}{\partial z} \left[\rho_a \frac{KK_{rg}}{\mu_g} \left(-\frac{\partial p_g}{\partial z} + \rho_g g_z \right) - D_m \frac{\partial p_a}{\partial z} \right] = 0 \end{aligned} \quad (7)$$

It is assumed that thermal equilibrium exists among the water, gas, and matrix at any location in the unsaturated packed bed. Considering the enthalpy transport, heat conduction, latent heat transport, and volumetric heat generation, the energy balance equation is represented by:

$$\begin{aligned} \frac{\partial}{\partial t} [(\rho C_p)_T T] + \frac{\partial}{\partial x} [\{ \rho_l C_{pl} u_l + (\rho_a C_{pa} + \rho_v C_{pv}) u_g \} T] \\ \frac{\partial}{\partial z} [\{ \rho_l C_{pl} w_l + (\rho_a C_{pa} + \rho_v C_{pv}) w_g \} T] + \\ H_v \dot{m} = \frac{\partial}{\partial x} \left[\lambda_{eff} \frac{\partial T}{\partial x} \right] + \frac{\partial}{\partial z} \left[\lambda_{eff} \frac{\partial T}{\partial z} \right] + Q \end{aligned} \quad (8)$$

where $(\rho C_p)_T T$ is the effective heat capacitance of the water-gas matrix mixture:

$$(\rho C_p)_T T = \rho_l C_{pl} \phi s + \rho_g C_{pg} \phi (1-s) + \rho_p C_{pp} (1-\phi)$$

$$\begin{aligned} \dot{m} = \frac{\partial}{\partial t} \{ \rho_v \phi (1-s) \} + \frac{\partial}{\partial x} \left[D_m \frac{\partial \rho_v}{\partial x} + \frac{\partial}{\partial z} \right] \\ - \frac{\partial}{\partial z} \left[\rho_v \frac{KK_{rg}}{\mu_g} \rho_g g_z - D_m \frac{\partial p_v}{\partial z} \right] \end{aligned}$$

$$\lambda_{eff} = \frac{0.80}{1 + 3.78 \exp^{-5.95s}}$$

$$Q = \omega \epsilon'_r E^2 = 2\pi f \epsilon_0 \epsilon'_r (\tan \delta) E_y^2$$

By applying the boundary conditions for solutions of the governing equations, these equations can be applied on a permeable surface, impermeable surface, or layer interface, as detailed below.

Permeable surface

Boundary conditions on a permeable surface (i.e., energy exchange at an open boundary) can be described as follows:

$$-\lambda_{eff} \frac{\partial T}{\partial z} = h_c (T - T_\infty) + \dot{m} H_v \quad (9)$$

Mass transfer at the permeable surface is modeled by a constant mass transfer coefficient, which is related to the local water vapor flux density:

$$\dot{m} = \rho_v w_v = h_m (\rho_v - \rho_{v\infty}) \quad (10)$$

where ρ_v is the density of water vapor at the permeable surface, and $\rho_{v\infty}$ is the reference vapor density in the gas phase surrounding the permeable surface. Therefore, the total pressure on the permeable surface can be defined as:

$$p_g = p_0 \quad (11)$$

Impermeable surface

The boundary condition at a closed impermeable boundary (i.e., symmetric, without heat or mass exchange) can be described by the following equations:

$$\frac{\partial T}{\partial x} = \frac{\partial T}{\partial z} = 0 \quad (12)$$

$$\frac{\partial u}{\partial x} = \frac{\partial u}{\partial z} = 0 \quad (13)$$

The simulated results for heat, multiphase flow, and pressure buildup in an unsaturated porous packed bed subjected to microwave energy are shown in Figs. 19

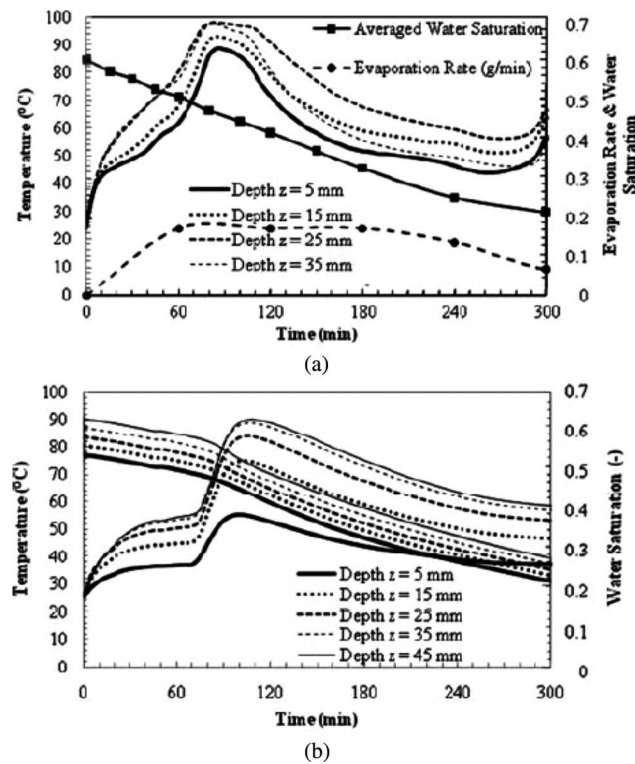


Figure 19. Temperature and water saturation profiles over time at different depths for the F-bed (sample thickness = 50 mm): (a) experimental and (b) simulated results. Reprinted from Suwannapum and Rattanadecho^[92] with permission from Taylor & Francis.

and 20. The temperature profiles of thin- and thick-layer packed beds are different, because the sample thickness affects the electromagnetic wave pattern inside the cavity and the sample (as explained in the previous section). Compared to a thick sample, a thin sample can more easily induce a resonance effect or strong standing wave, corresponding to a greater effect of the absorbed microwave power and the thermal energy transformation inside the sample.

Figure 20 shows the numerical results of the microwave power absorption profile as a function of time for a sample with a thickness of 5 cm. The temperature and microwave power absorption profile results are linked because the absorbed microwave power is mainly electromagnetic energy, which is transformed into thermal energy.

Figure 21 shows the temperature, water saturation, and pressure buildup distributions for an F-bed subjected to microwave heating for 10, 100, and 360 mins, respectively. The profiles displayed a wavy behavior. Regardless of thickness, all of the packed beds had cold- and hot-spot zones inside the samples.

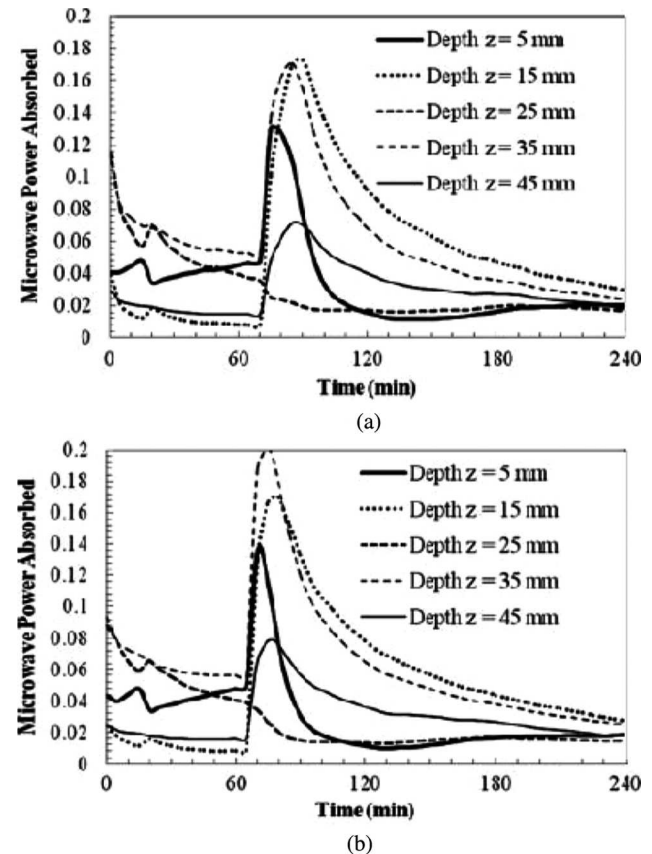


Figure 20. Microwave power absorption profiles overtime at different depths (sample thickness = 50 mm): (a) F- and (b) C-bed. Reprinted from Suwannapum and Rattanadecho^[92] with permission from Taylor & Francis.

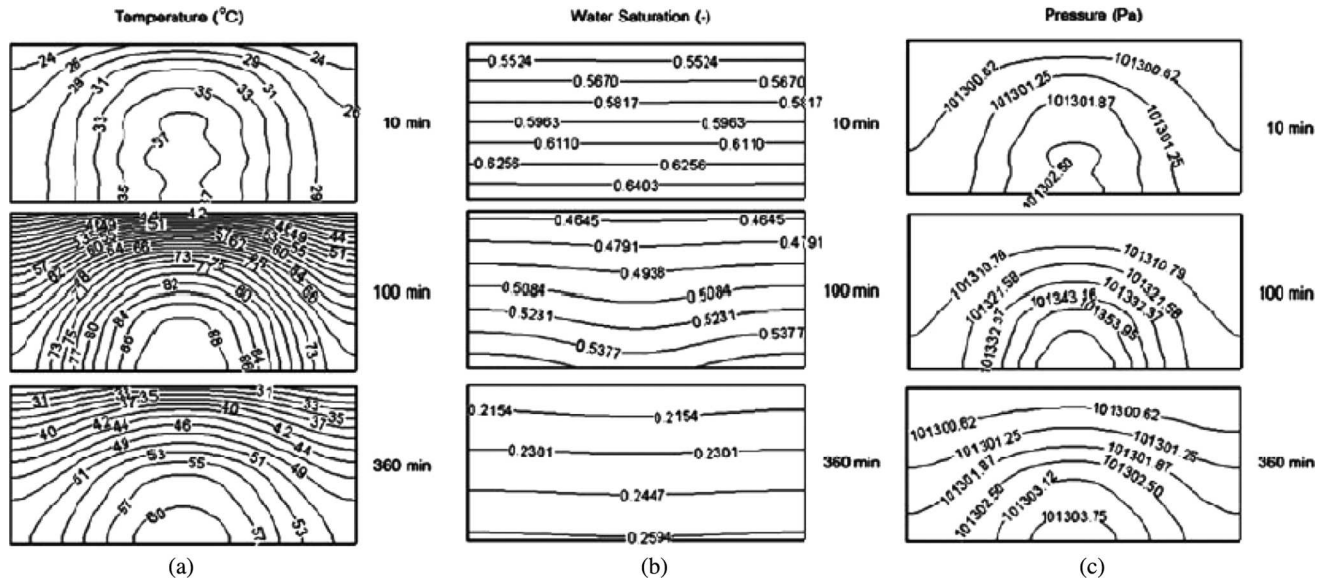


Figure 21. Contour plots for F-bed (50 mm) at drying times of 10, 100, and 360 min. (a) Temperature, (b) water saturation, and (c) pressure contours. Reprinted from Suwannapum and Rattanadecho^[92] with permission from Taylor & Francis.

Sungsoontorn et al.^[93] proposed a three-variable model by focusing on the microwave frequency, particle size, and electric-field intensity, to predict the heat and mass transfer and pressure build-up profiles in unsaturated porous media subjected to microwave energy. They employed a 1D analytical model for the MWD of the sample, utilizing Eqs. (14)–(16) in association with the boundary and initial conditions in Eqs. (17)–(19). Microwave energy absorption was assumed to decay exponentially into the sample following Lambert's law. This study focused on the absorbed microwave energy, temperature, and moisture distributions within the porous materials, as shown in Figs. 22–25, and discussed the multiphase flow behavior in detail. Variations in frequency, particle size, and electric field intensity were found to play important roles in the

overall drying kinetics. This research will serve as a fundamental tool for applications involving the MWD of porous media.

Energy conservation equation

$$\begin{aligned} & \frac{\partial}{\partial t} [(\rho C_p)_T T] + \frac{\partial}{\partial z} [\{\rho_l C_{pl} w_l + (\rho_a C_{pa} + \rho_v C_{pv}) w_g\} T] \\ &= \frac{\partial}{\partial z} \left(\frac{\partial T}{\partial z} \right) - H_v \left(\frac{\partial}{\partial t} (\rho_v \phi (1-s)) \right) + \frac{\partial}{\partial z} \\ & \times \left(\left(\rho_v \frac{K K_{rg}}{\mu_g} \left(\frac{\partial P_g}{\partial z} + \rho_g g_z \right) - \rho_g D_m \frac{\partial}{\partial z} \left(\frac{\rho_v}{\rho_g} \right) \right) \right) + Q \end{aligned} \quad (14)$$

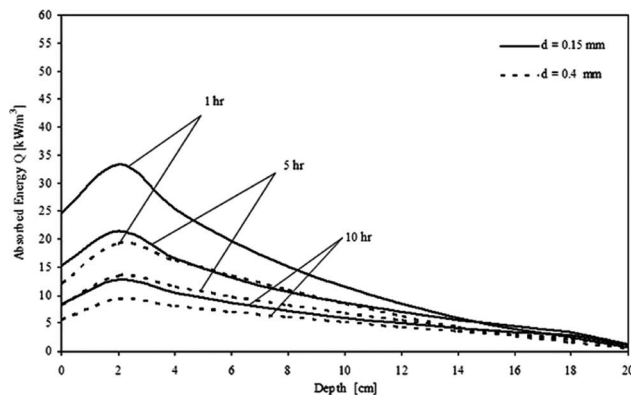


Figure 22. Energy-absorption profiles at various particle sizes ($f = 2.45$ GHz, $E_{in} = 4,200$ V/m, $S_{in} = 0.7$). Reprinted from Sungsoontorn et al.^[93] with permission from Taylor & Francis.

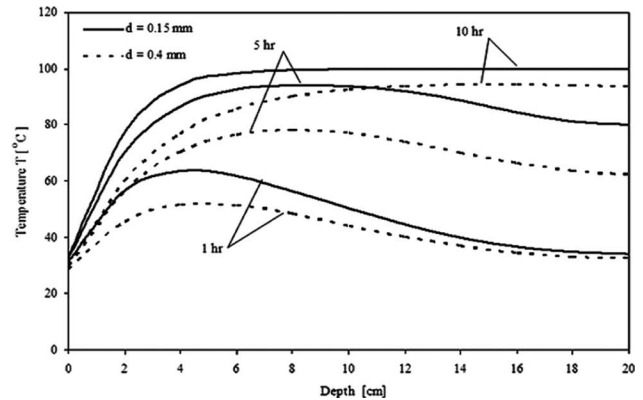


Figure 23. Temperature profiles at various particle sizes ($f = 2.45$ GHz, $E_{in} = 4,200$ V/m, $S_{in} = 0.7$). Reprinted from Sungsoontorn et al.^[93] with permission from Taylor & Francis.

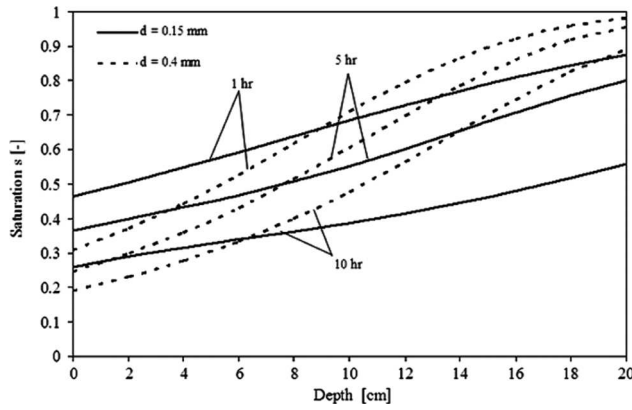


Figure 24. Moisture profiles at various particle sizes ($f = 2.45$ GHz, $E_{in} = 4,200$ V/m, $S_{in} = 0.7$). Reprinted from Sungsoontorn et al.^[93] with permission from Taylor & Francis.

Mass transport equation

$$\phi \frac{\partial}{\partial t} \left\{ s - Y_v(1 - s) + \frac{\partial}{\partial z} \left[\frac{KK_{rl}}{\mu_l} \left(\frac{\partial P_g}{\partial z} - \frac{\partial P_g}{\partial z} + g_z \right) + Y_v \frac{KK_{rg}}{\mu_g} \left(-\frac{\partial P_g}{\partial z} + \rho_g g_z \right) - Y_g D_m \frac{\partial}{\partial z} (W_v) \right] \right\} = 0 \quad (15)$$

Pressure build-up in porous media

$$\phi \frac{\partial}{\partial t} \left\{ Y_a(1 - s) + \frac{\partial}{\partial z} \left[Y_a \frac{KK_{rg}}{\mu_g} \left(-\frac{\partial P_g}{\partial z} + \rho_g g_z \right) - Y_g D_m \frac{\partial}{\partial z} \left(\frac{\rho_a}{\rho_g} \right) \right] \right\} = 0 \quad (16)$$

Boundary and initial conditions

$$-\lambda \frac{\partial T}{\partial z} = h_c(T - T_a) \quad (17)$$

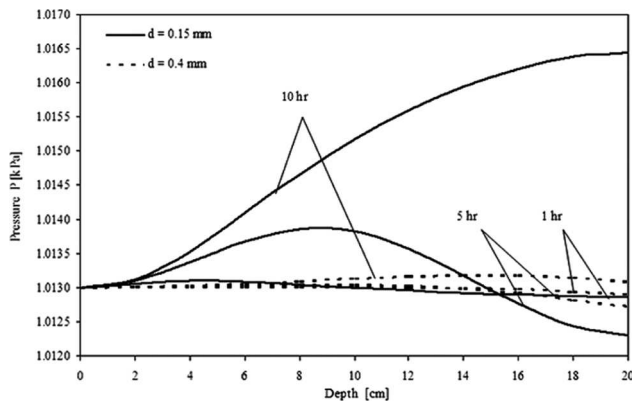


Figure 25. Pressure distribution at various particle sizes ($f = 2.45$ GHz, $E_{in} = 4,200$ V/m, $S_{in} = 0.7$). Reprinted from Sungsoontorn et al.^[93] with permission from Taylor & Francis.

$$\rho_l w_l + \rho_v w_v = h_m(\rho_v - \rho_{va}) \quad (18)$$

$$\frac{\partial T}{\partial x} = 0, \quad \frac{\partial w}{\partial z} = 0 \quad (19)$$

There have been many investigations of moisture transport during the intensive microwave heating of materials.^[94,95] Especially in biomaterials,^[96,97] microwaves are assumed to arrive at the open boundary where heat and moisture are convected away from the porous medium. Heat and moisture fluxes at the insulated closed boundary (right side) are zero and also to be a three-variable model, as shown in Fig. 26. Combining microwave with hot-air or infrared heating methods has been suggested to increase the surface temperature and remove accumulated surface moisture.

To maintain product quality, it is crucial to maintain a uniform heat distribution. Factors that influence the distribution of heat include factors related to the load (e.g., dielectric properties, load geometry, and mixture ratio) and the microwave system (e.g., turntable, operating frequency, placement inside the oven, oven size, and geometry). Several parameters must be known to account properly for all phenomena in a dielectric microwave heating process. These parameters include the distributions of the electromagnetic field, microwave power absorption, temperature, and multiphase flow. Understanding these parameters may require the researcher to solve coupled differential equations, including equations for moisture transport, pressure, energy, and the electromagnetic field.

Due to the complexity and number of equations involved, the numerical method is the only approach

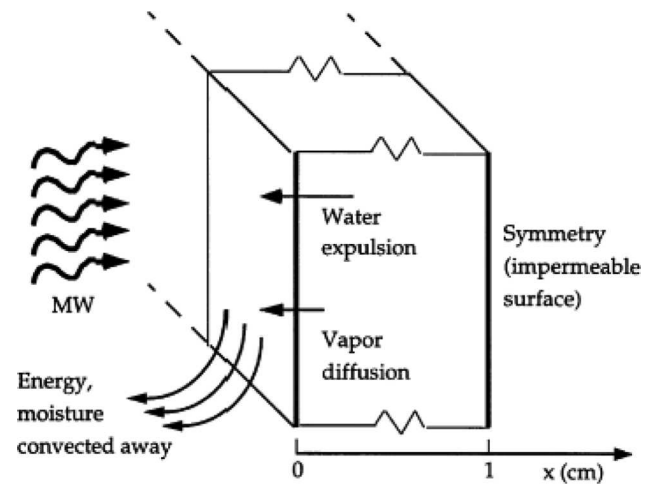


Figure 26. Schematic diagram of the heating process, with boundary conditions.^[86,96] Reprinted from *International Journal of Heat and Mass Transfer*, Vol. 42, H. Ni, A. K. Datta, and K. E. Torrance, "Moisture transport in intensive microwave heating of biomaterials: A multiphase porous media model," pp. 1501–1512, 1999, with permission from Elsevier.

that provides realistic simulations of the process. An attempt to solve these equations was carried out by Rakesh and Datta.^[97] They formulated a coupled transport and large deformation model for microwave puffing, which described the individual physics of the process in detail. As shown in Fig. 27, very high temperatures were required to generate the necessary pressures to puff the material. The process may not be successful unless carried out using an intensive heating source, such as a microwave.

Intermittent drying processes utilize time-varying heat input tailored to match the drying kinetics of the material being dried. Chua et al.^[98] overviewed the basic process of intermittent drying, selecting results from experiments and mathematical models for various biomaterials dried in a wide assortment of dryers. Intermittent drying can be performed by all types of batch dryers that employ time-varying operating conditions, including periodic or cyclic variations in pressure (from high to atmospheric), vacuum, temperature, or gas flow

rate. Intermittent drying is typically performed at low microwave frequencies. It is primarily applicable for materials that are heat sensitive or require long drying periods mainly or exclusively in the falling rate period. A slight-to-moderate increase in drying time should be expected with intermittent drying, but this disadvantage is compensated by a decrease in energy consumption and an enhancement in product quality.

From their finite element model (FEM) results of intermittent MWD, Zhang and Mujumdar^[99] recommended employing volumetric heating in a thermal drying process as a potential solution to diminish drying-induced stresses in grain kernels. The tempering period allows time for the internal moisture to distribute. Moisture and temperature gradients are equalized during the resting period when no heat or a reduced level of heat is provided. In the case of intermittent heating, the temperatures of the nodes do not increase constantly. The node temperatures are much lower than those in continuous heating, while the moisture

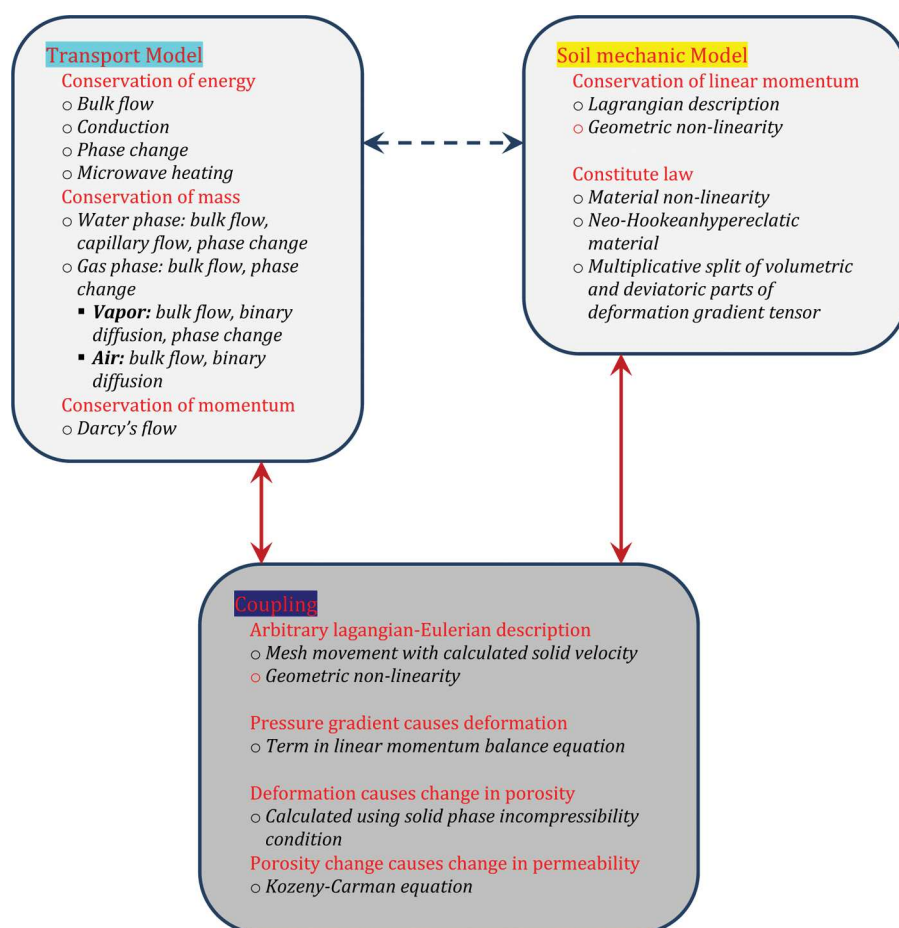


Figure 27. Components of the computational model, the different physical phenomena associated with the puffing process, and the coupling between the different physics. Reprinted from *Journal of Food Engineering*, Vol. 107, V. Rakesh and A.K. Datta, "Microwave puffing: Determination of optimal conditions using a coupled multiphase porous media—large deformation model," pp. 152–163, 2011, with permission from Elsevier.

potentials of different points of the body tend to be more uniform. This uniformity implies that the drying-induced stresses must also be decreased. For some heat-sensitive biological materials, intermittent drying should largely mitigate the problems caused by continuous hot-air drying, such as germinability, vigor, protein denaturation, and cracks.

Gong et al.^[100] performed a numerical study to understand the effects of intermittent microwave heating on the drying behavior of clay and its internal stress development. When intermittent microwave heating was used, the maximum tensile and compressive stresses within the dried clay were decreased significantly, and the time for the peak stresses to develop was somewhat reduced. Intermittent microwave heating also had a beneficial effect during the MWD of ceramics.^[101] Cracks were generated in the ceramic samples with continuous microwave heating. However, with a higher frequency of pulsation, crack formation could be avoided or delayed at lower moisture contents, although the sample did reach a higher temperature.

Gunasekaran^[102] verified the advantages of pulsed microwave-vacuum drying of cranberries, in terms of the energy efficiency and quality (color and texture) of the dried product. Energy efficiency and product quality improved with a longer ratio of the power-off to power-on time. Microwaves were operated at 5.33 and 10.67 kPa with power on for 1–6 cycles. These experimental results seemed to suggest that when the power-on time was shorter, more of the microwave energy was used to evaporate moisture, whereas when the power-on time was longer, the product temperature tended to increase, leading to a loss of quality of the heat-sensitive material.

The effect of intermittent MWD on shrinkage behaviors has been investigated.^[103,104] Experimental and numerical studies have reported that intermittent MWD improves the quality and temperature distribution of the dried food product. Sanga et al.^[105] presented experimental and numerical analyses of intermittent microwave-convection drying of heat-sensitive materials. Using fiber-optic probes, they tested the drying rate and temperature distribution of the product during drying. A diffusion model, which included temperature- and concentration-dependent diffusivity and allowed for shrinkage in an empirical fashion, yielded results that agreed with the measured drying rates. Their FEM may be applied to blends of wet solids with different loss factors for microwave energy absorption. Drying by intermittent microwave input to continuous convection drying provided a product with better quality (color) than continuous microwave input drying alone.

Chen et al.^[88] made a theoretical analysis of the effect of intermittent microwave heating patterns on the batch fluid drying of porous particles, considering uniform, sinusoidal, and rectangular patterns of microwave power. Under a constant electric field strength, they computed the temperature and moisture variations of apple particles in batch fluidized bed drying. Their results indicated the magnitude and distribution of the moisture, as well as the temperature and pressure within a particle.

Basak^[106] assessed the role of irradiation in the lateral and radial directions on the microwave heating of 2D cylinders for beef and oil samples. Their results revealed various resonance modes with lateral or radial irradiation and with samples having a large radius. The resonance modes corresponded to maxima in power and large processing rates. Hot-spot formation within a sample was a strong function of lateral/radial irradiation for various dielectrics of food. Radial irradiation was not favorable. In particular, a hot spot occurred with radial irradiation at the center of large oil samples, resulting in a larger thermal gradient. This finding was in contrast to earlier works, which established that radial irradiation minimizes the thermal gradient regardless of sample size.

Very recently, Chaiyo and Rattanadecho^[107] extended the work of Suwannapum and Rattanadecho,^[91] presenting a 2D numerical analysis of an unsaturated porous packed bed, which was placed in a rectangular waveguide and subjected to a combined microwave-vacuum system. The influences of vacuum pressure and microwave frequency on the temperature, absorbed microwave power, saturation distribution, pressure buildup distribution, and fluid movement within the porous media were investigated during drying. The effects on the overall drying kinetics were examined by selecting the dielectric properties as a function of moisture content and temperature. The microwave system was operated as a monochromatic wave of TE₁₀ mode (a dominant mode of electromagnetic propagation in a rectangular waveguide due to it has the lowest attenuation of all modes) at an operating frequency of 2.45 GHz. The magnetron-generated microwave energy was transmitted along the z-direction of the rectangular waveguide (inside dimensions: 110 × 54.61 mm) toward a water load situated at the end of the waveguide (see Fig. 28).

To model the physical single layer, the following assumptions were made:

- Because the microwave field in the TE₁₀ mode does not vary in direction between the broad faces, a 2D model over the *x*–*z* plane can be applied to analyze the electromagnetic field inside the rectangular waveguide.

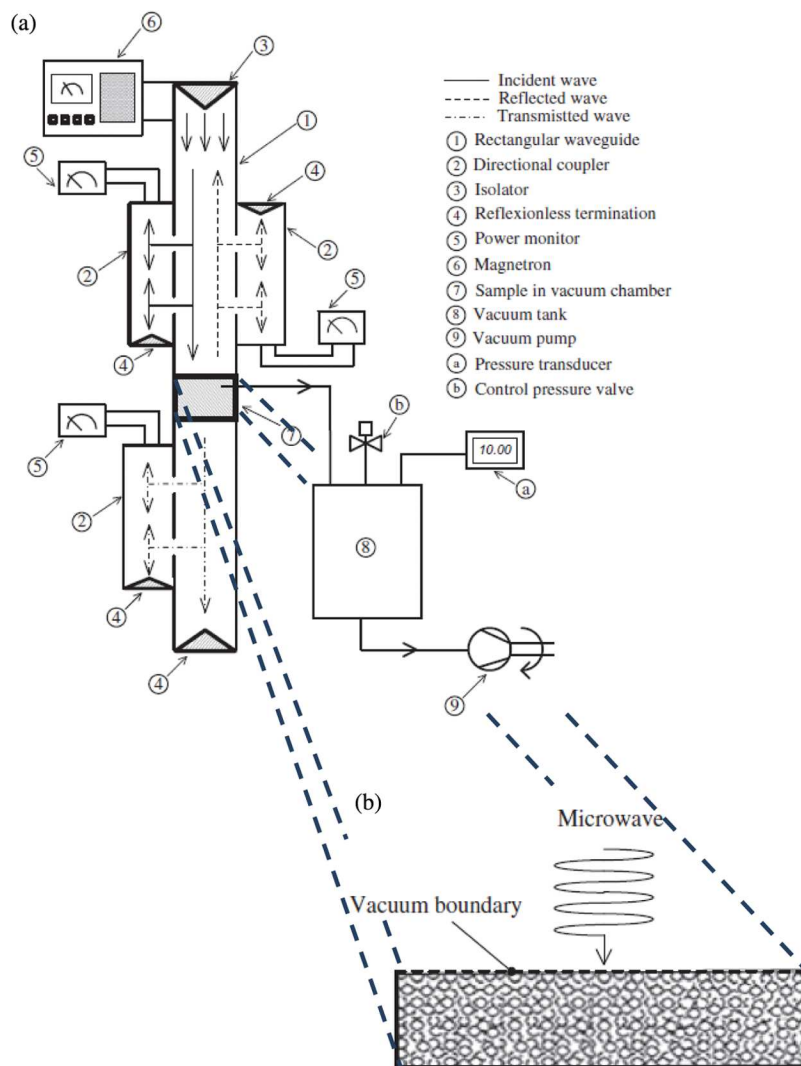


Figure 28. Schematic of (a) the combined microwave-vacuum system, and (b) the single-layer porous packed bed (sample) in a rectangular waveguide. Reprinted from *International Journal of Heat and Mass Transfer*, Vol. 65, K. Chaiyo and P. Rattanadecho, "Numerical analysis of heat-mass transport and pressure buildup of unsaturated porous medium in a rectangular waveguide subjected to a combined microwave and vacuum system," pp. 826–844, 2013, with permission from Elsevier.

- There is negligible absorption of microwave energy by the cavity (including air) in the rectangular waveguide.
- The walls of the rectangular waveguide are perfect conductors.
- The effect of the (quartz) sample container on the electromagnetic field can be neglected because it does not absorb microwave energy.

To obtain a closed set of governing macroscopic equations, the physical model shown in Fig. 29 was applied, and several simplifying assumptions were made:

1. The capillary porous material is rigid, and no chemical reactions occur in the sample.
2. Local thermodynamic equilibrium can be assumed.
3. Simultaneous heat and mass transport processes occur at a constant pressure. The dominant

mechanisms are capillary transport, vapor diffusion, and gravity. This situation is generally the case in the drying of capillary porous medium at a specified vacuum or atmospheric pressure when the temperature is lower than the boiling point.

4. The binary gas mixture of air and water vapor behaves like an ideal gas.
5. Darcy's law holds for the liquid and gas phases.
6. Gravity is included for the liquid and gas phases.
7. Permeability of liquid and gas can be expressed in terms of relative permeability.
8. The solid matrix is rigid and non-deformable.
9. In a macroscopic sense, the porous packed bed is homogeneous and isotropic, and water is not bound to the solid matrix. Thus, the volume average model for a homogeneous and isotropic material can be used in the theoretical modeling and analysis.

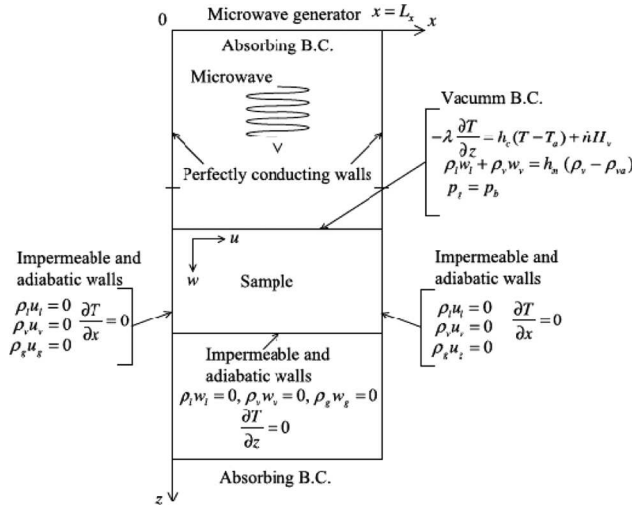


Figure 29. Physical single-layer model. Reprinted from *International Journal of Heat and Mass Transfer*, Vol. 65, K. Chaiyo and P. Rattanadecho, "Numerical analysis of heat-mass transport and pressure buildup of unsaturated porous medium in a rectangular waveguide subjected to a combined microwave and vacuum system," pp. 826–844, 2013, with permission from Elsevier.

- Similar to the electromagnetic field, the temperature and moisture profiles can be assumed to be 2D in the x - z plane.

Moisture transport equation

$$\phi \frac{\partial}{\partial t} [\rho_l s + \rho_v (1-s)] + \frac{\partial}{\partial t} [\rho_l u_l + \rho_v u_v] + \frac{\partial}{\partial t} [\rho_l w_l + \rho_v w_v] = 0 \quad (20)$$

Total pressure equation

$$\phi \frac{\partial}{\partial t} [\rho_a (1-s)] + \frac{\partial}{\partial x} \left[\rho_a \frac{KK_{rg}}{\mu g} \left(-\frac{\partial P_g}{\partial x} \right) - D_m \frac{\partial}{\partial z} \rho_a \right] + \frac{\partial}{\partial z} \left[\rho_a \frac{KK_{rg}}{\mu g} \left(-\frac{\partial P_g}{\partial z} + \rho_g g_z \right) - D_m \frac{\partial}{\partial z} \rho_a \right] = 0 \quad (21)$$

Heat transport equation

$$\rho C_p \frac{\partial T}{\partial t} + \frac{\partial}{\partial x} [\{\rho_l C_{pl} u_l + (\rho_a C_{pa} + \rho_v) u_g\} T] + \frac{\partial}{\partial z} [\{\rho_l C_{pl} w_l + (\rho_a C_{pa} + \rho_v C_{pv}) w_g\} T] + H_v \dot{n} = \frac{\partial}{\partial x} \left[\lambda_{eff} \frac{\partial T}{\partial x} \right] + \frac{\partial}{\partial z} \left[\lambda_{eff} \frac{\partial T}{\partial z} \right] + Q \quad (22)$$

where ρC_p is the effective heat capacitance of the water-gas matrix mixture:

$$\rho C_p = \rho_l C_{pl} \phi s + (\rho_a C_{pa} + \rho_v C_{pv}) \phi (1-s) + \rho_p C_{pp} (1-\phi) \quad (23)$$

The phase change term is given by

$$\dot{n} \frac{\partial}{\partial t} \{ \rho_v \phi (1-s) \} + \frac{\partial}{\partial x} \left[-D_m \frac{\partial \rho_v}{\partial x} \right] + \frac{\partial}{\partial z} \left[\rho_v \frac{KK_{rg}}{\mu_g} \rho_g g_z - D_m \frac{\partial \rho_v}{\partial z} \right] \quad (24)$$

Figures 30–32 show the temperature profile at various times under atmospheric pressure and a vacuum pressure of 13.3 kPa. The temperature inside the drying sample was higher under MWD than conventional drying, whereas the surface temperature stayed cooler due

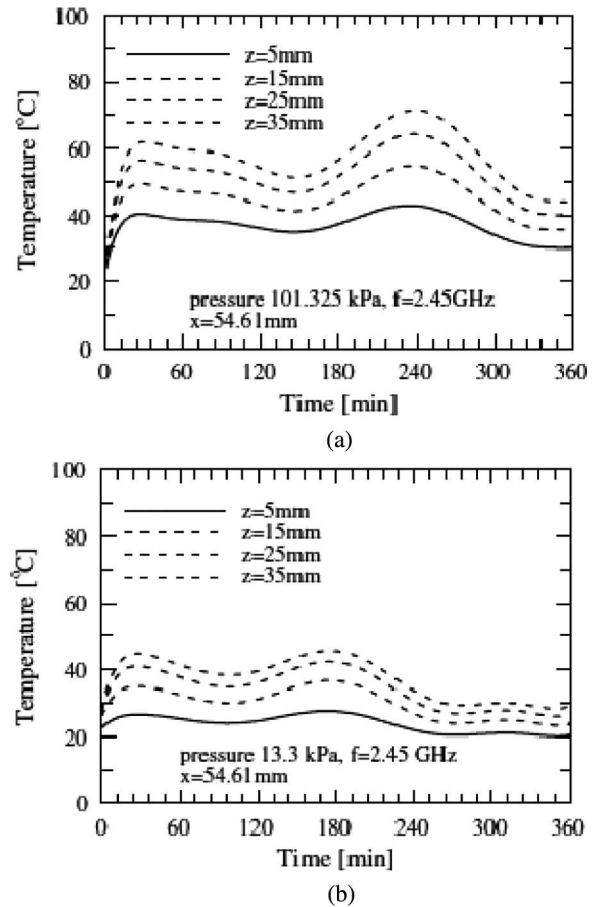


Figure 30. Temperature profile overtime at different z -depths (x -width = 54.61 mm): (a) atmospheric pressure, (b) vacuum pressure of 13.3 kPa. Reprinted from *International Journal of Heat and Mass Transfer*, Vol. 65, K. Chaiyo and P. Rattanadecho, "Numerical analysis of heat-mass transport and pressure buildup of unsaturated porous medium in a rectangular waveguide subjected to a combined microwave and vacuum system," pp. 826–844, 2013, with permission from Elsevier.

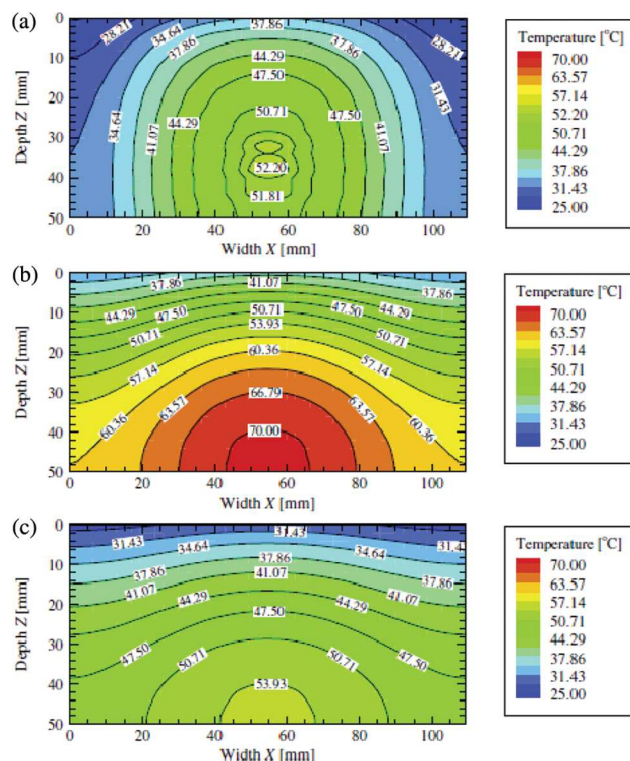


Figure 31. Temperature distribution inside the sample at atmospheric pressure and a microwave frequency of 2.45 GHz. (a) $t = 10$ min, (b) $t = 100$ min, and (c) $t = 360$ min. Reprinted from *International Journal of Heat and Mass Transfer*, Vol. 65, K. Chaiyo and P. Rattanadecho, "Numerical analysis of heat-mass transport and pressure buildup of unsaturated porous medium in a rectangular waveguide subjected to a combined microwave and vacuum system," pp. 826–844, 2013, with permission from Elsevier.

to effect of the surrounding air. Evaporation occurred at a lower temperature at the sample surface, due to evaporative cooling.

Chaiyo and Rattanadecho^[107] numerically determined the heat, multiphase flow, and pressure buildup distributions in an unsaturated porous packed bed subjected to microwave energy under atmospheric pressure or a vacuum pressure of 13.3 kPa (100 Torr). Figure 33 shows the electric-field distribution along the center axis ($x = 54.61$ mm) of the rectangular waveguide when inserted into the sample at different drying times ($t = 10, 100$, and 360 min). Because the sample was composed of glass beads, water, and air, it can be assumed to be a lossy (moist and porous) material. Under atmospheric pressure, the resonance of the standing wave configuration inside the sample was weak compared to the left-hand side of the sample, as shown in Figs. 33b and 33c. For the electric-field distribution inside the cavity (left-hand side), a stronger standing wave with a large amplitude was formed by interference between the incident and reflected waves from the

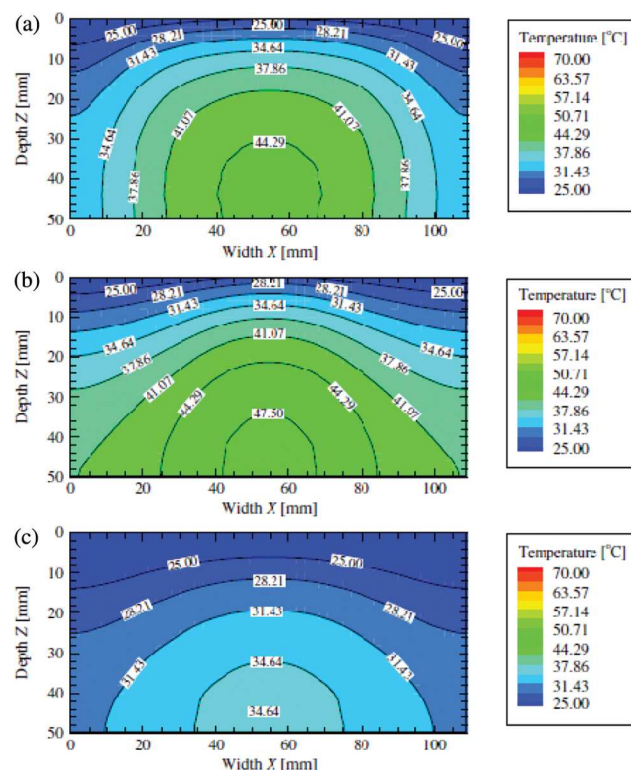


Figure 32. Temperature distribution inside the sample at a vacuum pressure of 13.3 kPa and a microwave frequency of 2.45 GHz: (a) $t = 10$ min, (b) $t = 100$ min, and (c) $t = 360$ min. Reprinted from *International Journal of Heat and Mass Transfer*, Vol. 65, K. Chaiyo and P. Rattanadecho, "Numerical analysis of heat-mass transport and pressure buildup of unsaturated porous medium in a rectangular waveguide subjected to a combined microwave and vacuum system," pp. 826–844, 2013, with permission from Elsevier.

sample surface, due to the different dielectric properties of the materials (air and sample) at the interface.

For the case of highly deformable products, Perré and May^[108] proposed a numerical drying model that accounts for the coupling between transfer and solid mechanics. To describe the drying of porous media that undergo large deformations due to shrinkage, they modified their previous *TransPore* model.^[109] In the resultant Model 2, the porous medium is described with two independent variables (temperature and moisture content or equivalent variables). This model can be analyzed as a simplification of Model 3. This model does not account for the internal gaseous pressure. Darcy's law includes only the liquid phase, in which capillary forces are the sole actors. The model assumes that capillary pressure is a function of moisture content alone (rather than moisture and temperature). This approach is worthwhile because it enables the most important feature of drying (i.e., coupling between heat and mass transfer) to be analyzed, as shown in Eqs. (25) and (26). This article presents a typical example of this

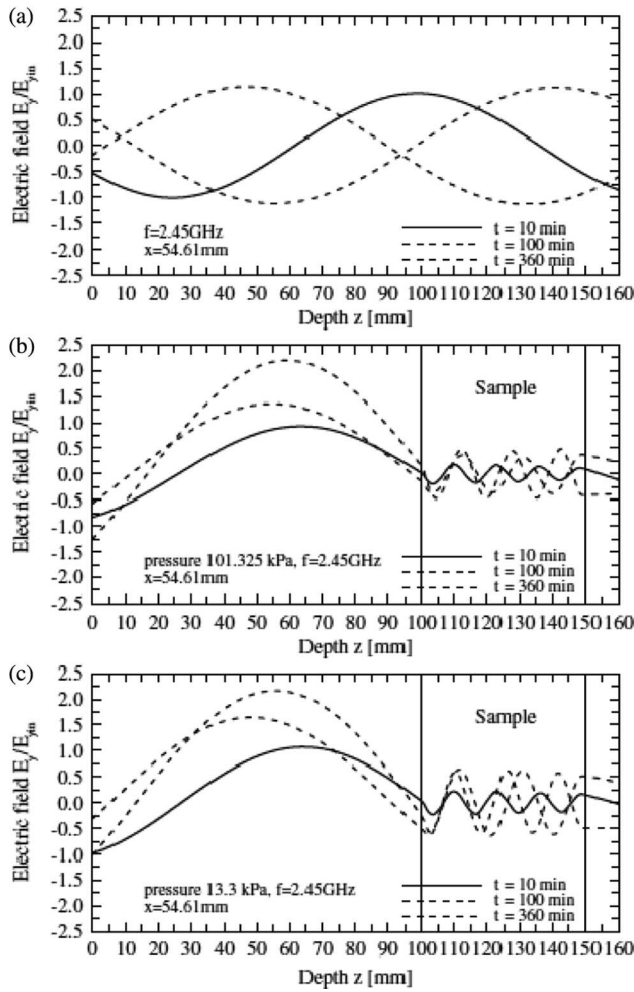


Figure 33. Electric-field distribution a at microwave frequency of 2.45 GHz. (a) Empty rectangular waveguide. (b–c) Sample in the rectangular waveguide at (b) 101.325 kPa or (c) 13.3 kPa. Reprinted from *International Journal of Heat and Mass Transfer*, Vol. 65, K. Chaiyo and P. Rattanadecho, “Numerical analysis of heat-mass transport and pressure buildup of unsaturated porous medium in a rectangular waveguide subjected to a combined microwave and vacuum system,” pp. 826–844, 2013, with permission from Elsevier.

model for potato. The computed results reveal dramatic variations of the sample shape as water is removed from the product. Due to exchange surface reduction, the drying rate decreases, even though free water remains available at the surface, as shown in Fig. 34.

Water conservation

$$\frac{\partial}{\partial t}(\rho_s X) + \nabla \cdot (\bar{q}_v) + \nabla \cdot (\bar{q}_l) = 0 \quad (25)$$

with

$$\bar{q}_v = -\rho_v \bar{K}_v \nabla X; \quad \bar{q}_l = -\rho_l \bar{K}_l \nabla X$$

Energy conservation

$$\begin{aligned} \frac{\partial}{\partial t}[\rho_s(h_0 + Xh_l)] + \nabla \cdot (\rho_l h_l \bar{q}_l + \rho_v h_v \bar{q}_v) \\ = \nabla \cdot (\bar{\lambda}_{eff} \nabla T) + \Phi \end{aligned} \quad (26)$$

Perre and Turner’s *TransPore* model,^[109] which was based on a discussion by Whitaker,^[83] was proposed as a comprehensive heat and mass transfer computational model for simulating the drying of porous media. The necessary governing equations are summarized as follows:

Liquid conservation equation

$$\begin{aligned} \frac{\partial}{\partial t}(\varepsilon_w \rho_w + \varepsilon_g \rho_g + \bar{\rho}_b) + \nabla \cdot (\rho_w \bar{v}_w + \rho_v \bar{v}_v \\ + \bar{\rho}_b \bar{v}_b) = \nabla \cdot (\rho_g \bar{D}_{eff} \nabla \omega_v) \end{aligned} \quad (27)$$

Energy conservation equation

$$\begin{aligned} \frac{\partial}{\partial t}(\varepsilon_w \rho_w h_w + \varepsilon_g(\rho_v h_v + \rho_a h_a) + \bar{\rho}_b \bar{h}_b) + \rho_0 h_s - \varepsilon_g P_g \\ \times \nabla \cdot (\rho_w h_w \bar{v}_w + (\rho_v h_v + \rho_a h_a) \bar{v}_g + h_b \bar{\rho}_b h v_b) \\ = \nabla \cdot \left((\rho_g \bar{D}_{eff}((h_v \nabla \omega_v + h_a \nabla \omega_a)) + \bar{K}_{eff} \nabla T) \right) + \Phi \end{aligned} \quad (28)$$

Air conservation equation

$$\frac{\partial}{\partial t}(\varepsilon_g \rho_g) + \nabla \cdot (\rho_a \bar{v}_a) = \nabla \cdot (\rho_g \bar{D}_{eff} \nabla \omega_a) \quad (29)$$

where the gas and liquid phase velocities are given by the Generalized Darcy’s Law:

$$\bar{v}_l = -\frac{\bar{K} \bar{k}}{\mu_l} \nabla \phi_l, \quad \nabla \phi_l = \nabla P_l - \rho_l g \nabla \chi \quad \text{where } l = w, g \quad (30)$$

The authors demonstrated that their drying model is capable of handling the comprehensive set of macroscopic equations in three spatial dimensions. For example, the evolution of the average moisture content, center temperature, and center pressure over time are depicted in Fig. 35 for concrete and in Fig. 36 for softwood.

Nonthermal equilibrium model for microwave drying

In 2012, Rattanadecho and Klinbun^[110] numerically investigated the natural convection of fluid in saturated

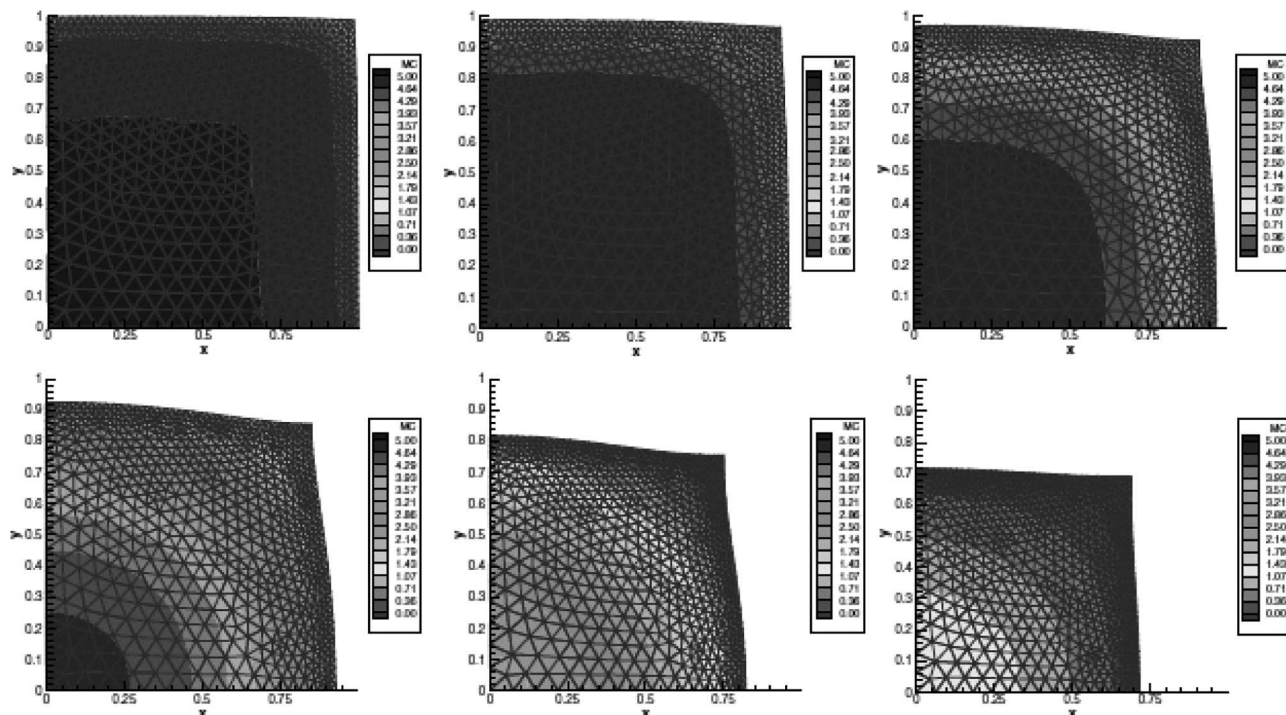


Figure 34. Shape and moisture content iso-values of the shipped section during 1, 2, 5, 10, 20, and 30 h of drying. Mass diffusivity $= 3 \times 10^{-10} \text{ m}^2/\text{s}$. Reprinted from Perré and May^[108] with permission from Taylor & Francis.

porous media under an electromagnetic field. The influences of material properties, microwave power levels, and operating frequencies on the transport processes in porous media were numerically analyzed. By assuming that the porous medium consists of water

and spherical solid particles, solving the Brinkman–Forchheimer extended Darcy model for the momentum equation is employed, and two energy equations with local thermal nonequilibrium (LTNE) models. Figure 37 showed a schematic diagram of the problem. The container was filled with a saturated porous medium. The

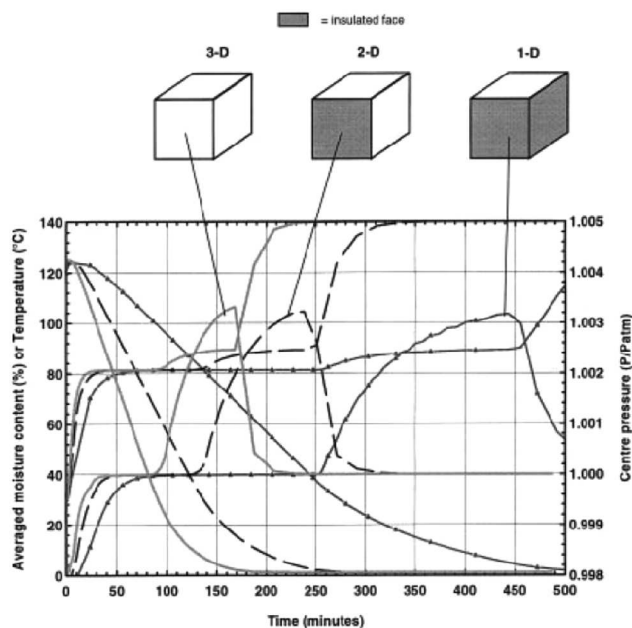


Figure 35. Numerical simulation of concrete drying (140/80°C for dry/wet bulk), showing the effect of the number of spatial dimensions on the overall drying curves. Reprinted from Perré and May^[108] with permission from Taylor & Francis.

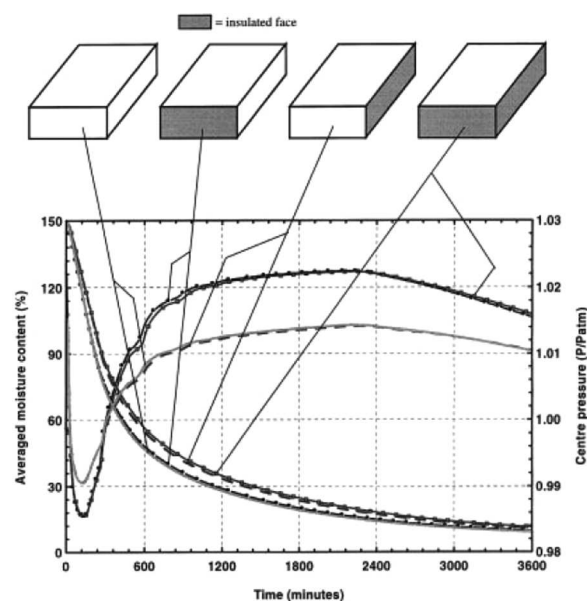


Figure 36. Low-temperature drying of softwood (80/50°C for dry/wet bulk), showing the overall drying and internal pressure curves for different exchange surface configurations. Reprinted from Perré and May^[108] with permission from Taylor & Francis.

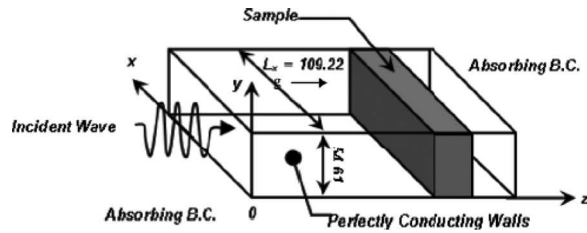


Figure 37. Model geometry of the single-slot MCA. Reprinted from Rattanadecho and Klinbun^[110] with permission from Taylor & Francis.

porous medium consisted of water and spherical solid. The results indicated that the phenomena taking place inside the saturated porous media in electromagnetic wave drying processes using LTNE and local thermal equilibrium (LTE) models. Figures 38a and 38b show the temperature distributions of the solid and fluid phases at various power input levels, along with the horizontal axis ($z = 10$ mm) and vertical axis ($x = 54.61$ mm) of a rectangular waveguide, respectively. For water-glass beads, the porous packed bed with $P = 1,000$ W corresponded to a higher temperature than that for the porous packed bed with $P = 300$ W for x and z directions. This was due to the high power input, which affected the local electromagnetic heat generation (Q) and thus created the temperature difference.

That same year, Klinbun and Rattanadecho published a second article,^[111] in which they numerically studied the heating of a multilayer porous packed bed that was subjected to microwave radiation with a rectangular waveguide.

Keagin and Rattanadecho^[112] presented a valuable study on local thermal non-equilibrium (LTNE) in porous material, in the context of microwave ablation

(MWA). This research was a preliminary investigation on the effect of phase change due to water evaporation for the future work. In the MWA process, heat from microwave energy is applied to kill cancer cells without damaging the surrounding tissue. These authors investigated the transient distribution of tissue and blood temperatures within porous liver during MWA, using an LTNE model-based single-slot microwave coaxial antenna (MCA). Given the highly complicated tumor structure, the authors simplified the model geometry of the single-slot MCA, as shown in Figs. 39 and 40. These studies^[110–112] can be used to extend MWD modeling and have been continuously developing by the authors.

To analyze electromagnetic wave propagation and heat transfer within the porous liver during the MWA process, the authors numerically solved the system of governing equations, initial conditions, and boundary conditions using the FEM via COMSOL Multiphysics. The boundary conditions are described in Fig. 41. To analyze the electromagnetic wave propagation, the following assumptions and relevant equations were used:

1. Electromagnetic wave propagation can be modeled in 2D axially symmetrical cylindrical coordinates ($r-z$).
2. An electromagnetic wave propagating in an MCA is characterized by transverse electromagnetic fields.
3. An electromagnetic wave in porous liver is characterized by transverse magnetic fields.
4. The wall of an MCA is a perfect electric conductor.
5. The outer surface of the porous liver is truncated by a scattering boundary condition.
6. The dielectric properties of the porous liver are uniform and constant.

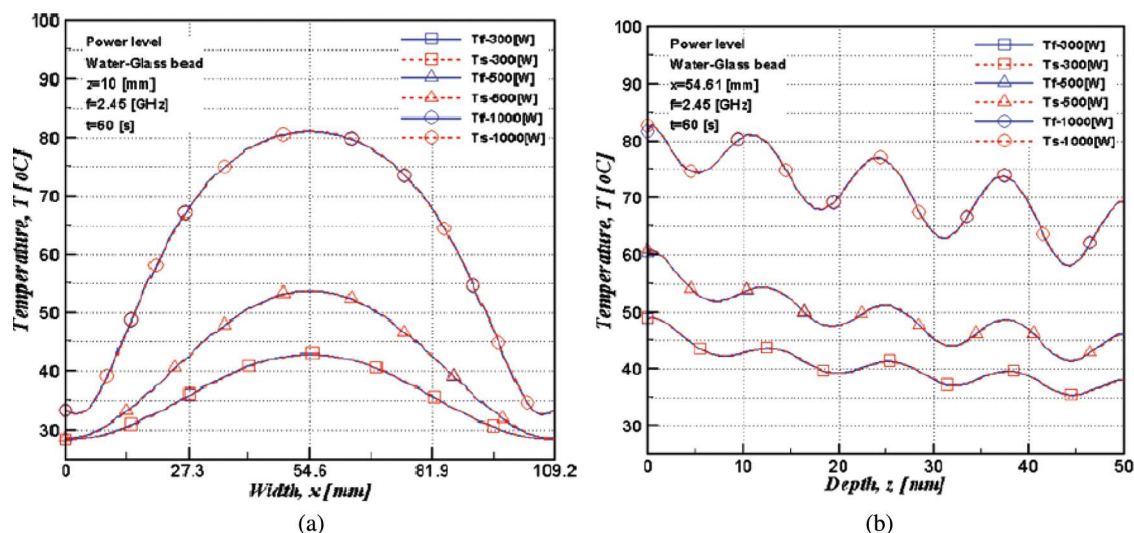


Figure 38. Temperature distributions of the solid and fluid phases at various power input levels: (a) along the x -axis and (b) along the z -axis. Reprinted from Rattanadecho and Klinbun^[110] with permission from Taylor & Francis.

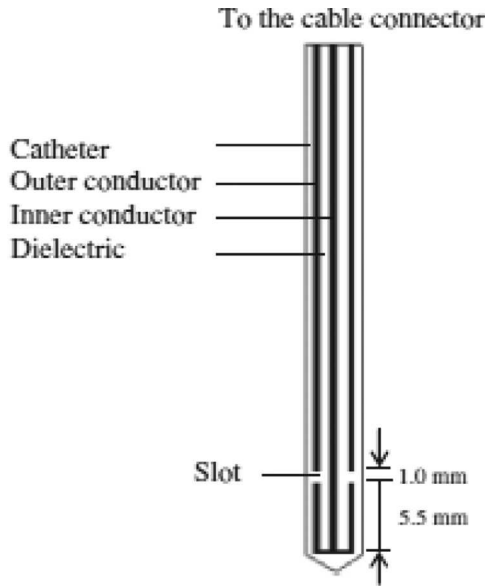


Figure 39. Model geometry of the single-slot MCA. Reprinted from *International Journal of Heat and Mass Transfer*, Vol. 67, P. Keangin and P. Rattanadecho, "Analysis of heat transport on local thermal non-equilibrium in porous liver during microwave ablation," pp. 46–60, 2013, with permission from Elsevier.

Electric field equation

$$\vec{E} = e_r \frac{C}{r} e^{j(\omega t - kz)}, C = \sqrt{\frac{ZP}{\pi \cdot \ln(r_{\text{outer}}/r_{\text{inner}})}} \quad (31)$$

Magnetic field equation

$$\vec{E} = e_\phi \frac{C}{rZ} e^{j(\omega t - kz)}, C = \sqrt{\frac{ZP}{\pi \cdot \ln(r_{\text{outer}}/r_{\text{inner}})}} \quad (32)$$

Wave equation

$$\nabla \times \left(\left(\epsilon_r - \frac{j\sigma}{\omega\epsilon_0} \right)^{-1} \nabla \times \frac{\vec{H}}{\phi} \right) - \mu_r k_0^2 \frac{\vec{H}}{\phi} = 0 \quad (33)$$

Boundary conditions

$$\vec{E}_r = 0, \frac{\partial \vec{E}}{\partial r} = 0 \text{ and } \hat{n} \times \vec{E} = 0 \quad (34)$$

To analyze the heat transfer, tissue and blood temperatures within the porous liver during the MWA process were obtained by solving two energy equations, assuming LTNE and including the microwave power absorbed. To simplify the problem, the following assumptions were made:

1. Corresponding to electromagnetic wave propagation analysis, blood flow and heat transfer can be modeled in 2D axially symmetrical cylindrical coordinates (r - z).
2. Porous liver is homogenous, thermally isotropic, and saturated with a fluid (blood).

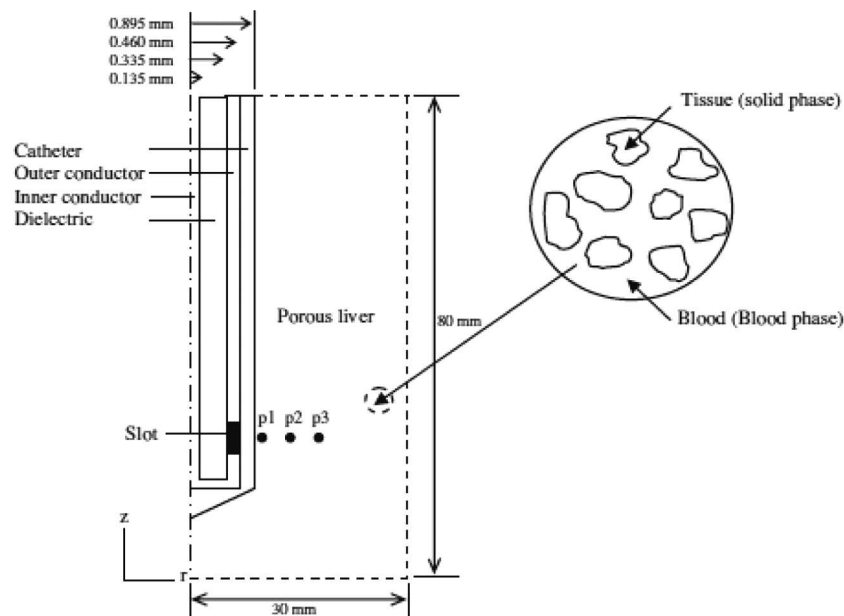


Figure 40. Axially symmetrical model geometry. Three positions of the slot center, p1 (2.5 mm, 16 mm), p2 (4.5 mm, 16 mm), and p3 (8.5 mm, 16 mm), are used to determine the tissue and blood temperatures. Reprinted from *International Journal of Heat and Mass Transfer*, Vol. 67, P. Keangin and P. Rattanadecho, "Analysis of heat transport on local thermal non-equilibrium in porous liver during microwave ablation," pp. 46–60, 2013, with permission from Elsevier.

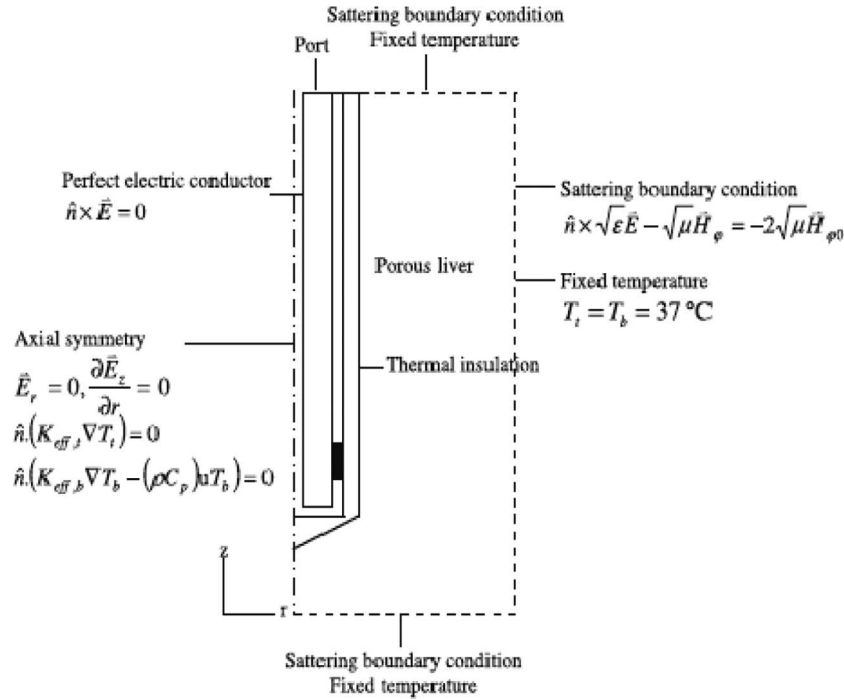


Figure 41. Boundary condition for analysis of electromagnetic wave propagation and heat transfer. Reprinted from *International Journal of Heat and Mass Transfer*, Vol. 67, P. Keangin and P. Rattanadecho, "Analysis of heat transport on local thermal non-equilibrium in porous liver during microwave ablation," pp. 46–60, 2013, with permission from Elsevier.

3. Blood flow is incompressible and Newtonian.
4. No phase change occurs within the porous liver, no energy exchange occurs through the outer surface of the porous liver, and no chemical reactions occur within the porous liver.
5. The porosities and thermal properties of the porous liver are constant.

Governing equations describing the heat-transfer phenomena for tissue and blood phases, incorporating the LTNE conditions, can be represented as follows:

Tissue phase equation

$$(1 - \phi)(\rho C_p)_t \frac{\partial T_t}{\partial t} = \nabla \cdot (K_{t,eff} \nabla T_t) - h_{tb} a_{tb} (T_t - T_b) - \omega_b C_b (T_t - T_b) + (1 - \phi) Q_{met} + (1 - \phi) Q_{ext,t} \quad (35)$$

Blood phase equation

$$\phi(\rho C_p)_b \left(\frac{\partial T_b}{\partial t} + u \cdot \nabla T_b \right) = \nabla \cdot (K_{b,eff} \nabla T_b) + h_{tb} a_{tb} (T_t - T_b) + \omega_b C_b (T_t - T_b) + \phi Q_{ext,b}$$

where

$$K_{t,eff} = (1 - \phi) K_t, K_{b,eff} = \phi K_b$$

The temperature profile formed a nearly ellipsoidal shape around the slot. The temperature was highest

near the MCA slot and decreased with distance from the MCA. In the three analyzed cases, the temperature profiles increased with increasing heating time. At locations far from the MCA, the temperatures of tissue and blood from LTNE models and of tissue from local thermal equilibrium models approached the initial temperature of 37°C, as shown in Fig. 42.

Energy and exergy analyses

The main target of designing and optimizing commercial drying processes is to reduce the amount of moisture in a product to a desired value, while utilizing as little energy as possible. Consequently, the energy quantity and quality as well as heat and mass transfer should be evaluated throughout the drying process.^[113,114] Exergy is a measurement of the maximum useful work that can be done by a system interacting with an environment at a constant pressure and temperature. Exergy analysis has been increasingly accepted as a useful tool in the design, assessment, optimization, and improvement of energy systems.

For example, Jindarat et al.^[56] experimentally investigated the energy consumption during the drying of non-hygroscopic porous packed beds by an industrial CMCB, as shown in Fig. 6, accounting for the effects of drying time, hot-air temperature, porous structure (F- or C-bed), and magnetron location on the overall

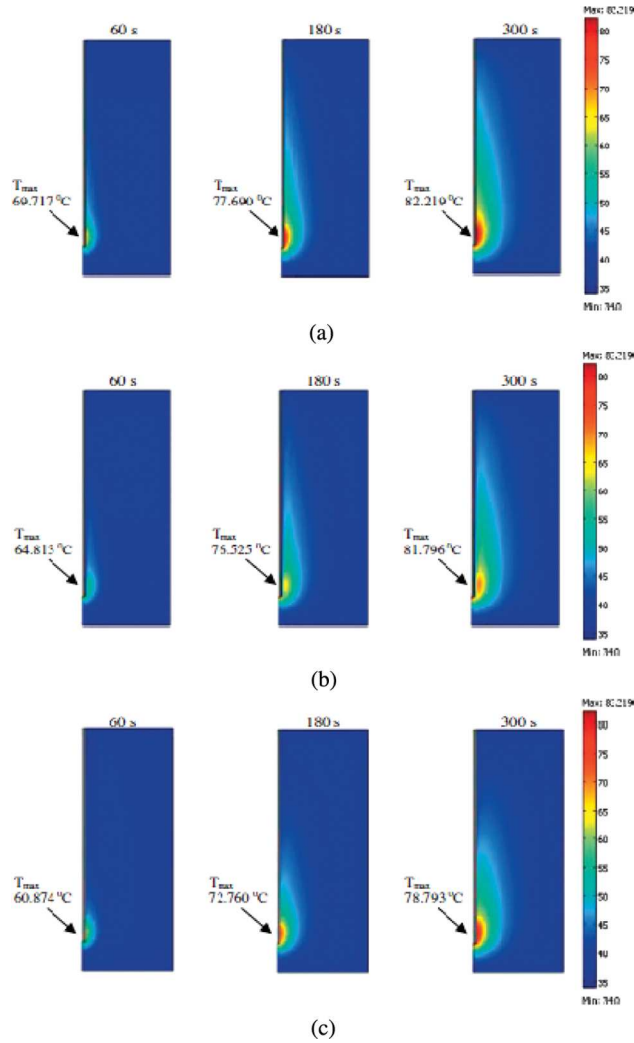


Figure 42. Temperature profiles in the porous liver at various times. (a) Tissue and (b) blood temperature profiles of the LTNE model. (c) Tissue temperature profiles of the local thermal equilibrium model based on the same condition in the figure. Reprinted from *International Journal of Heat and Mass Transfer*, Vol. 67, P. Keangin and P. Rattanadecho, "Analysis of heat transport on local thermal non-equilibrium in porous liver during microwave ablation," pp. 46–60, 2013, with permission from Elsevier.

drying kinetics and energy consumption. A schematic of the conservation of mass for the control volume of the cavity is shown in Fig. 43.

The mass balance equation can be defined as in Eq. (37):

$$\frac{dm_{cv}}{dt} = \dot{m}_{g1} - \dot{m}_{g2} \quad (37)$$

where \dot{m}_{g1} and \dot{m}_{g2} are the mass flow rates at inlet (1) and exit (2), respectively. The energy efficiency (η_e) for the drying process is defined as:

$$\eta_e = \frac{W_d [h_{fg}(M_{p1} - M_{p2}) + c_m(T_{m2} - T_{m1})]}{\dot{m}(h_1 - h_0)\Delta t + \Delta t \dot{Q}_{mw}} \quad (38)$$

where W_d is the weight of dried material; h_{fg} is the latent heat of vaporization; M_{p1} and M_{p2} are the particle moisture content on a dry basis at inlet (1) and exit (2), respectively; c_m is the specific heat of the material; T_{m1} and T_{m2} are the temperature at inlet (1) and exit (2), respectively; \dot{m} is the mass flow rate; Δt is the time; and \dot{Q}_{mw} is the microwave energy.

Figures 44–47 show the temperature and moisture variations as a function of time for the C- and F-beds with a constant initial moisture content of 25% (dry basis). In the CMCB at 30°C and 70°C, the moisture profiles of the sample continuously decreased at a faster rate compared to convective drying alone. Thus, the bulk of the sample absorbed the largest amount of microwave energy, which corresponds to the level of absorbed energy in the sample. These findings demonstrate the potential of a technique combining conventional and microwave heating with a continuous belt system to reduce electrical energy consumption. If implemented in industry, this system would decrease production costs by reducing electrical energy consumption.

Prommas et al.^[44] investigated the effects of the drying time, hot-air temperature, porous structure

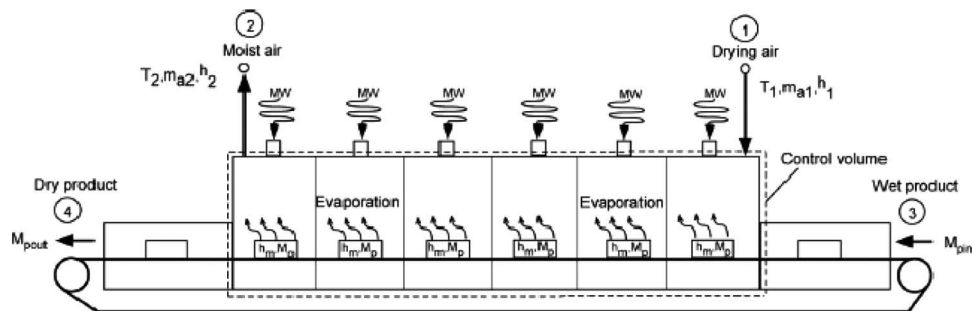


Figure 43. Schematic of the control volume during a drying process in a CMCB. Reprinted from Jindarat et al.^[56] with permission from Taylor & Francis.

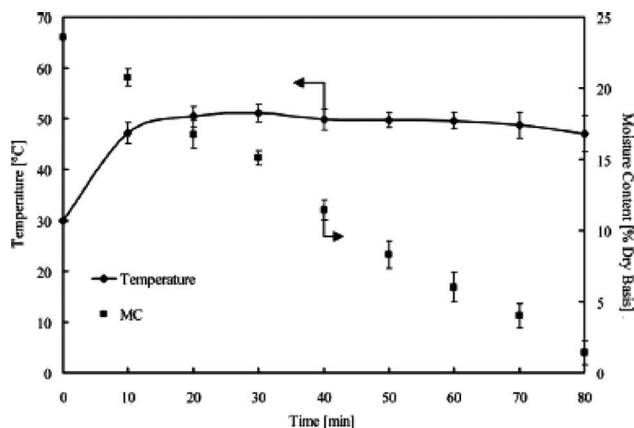


Figure 44. Variations in temperature and moisture over time for drying in the CMCB ($T_1 = 30^\circ\text{C}$, case 1, C-bed). Reprinted from Jindarat et al.^[56] with permission from Taylor & Francis.

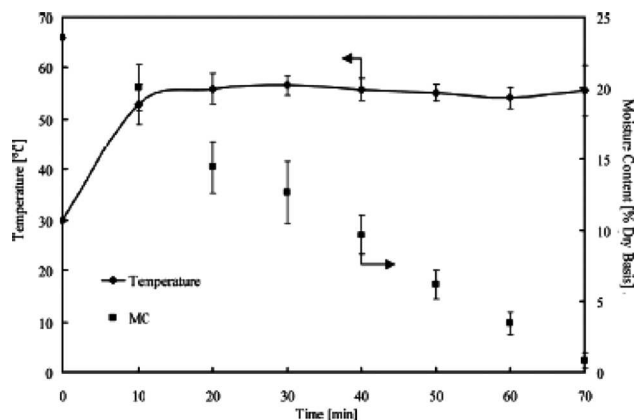


Figure 47. Variations in temperature and moisture over time for drying in the CMCB ($T_1 = 70^\circ\text{C}$, case 4, C-bed). Reprinted from Jindarat et al.^[56] with permission from Taylor & Francis.

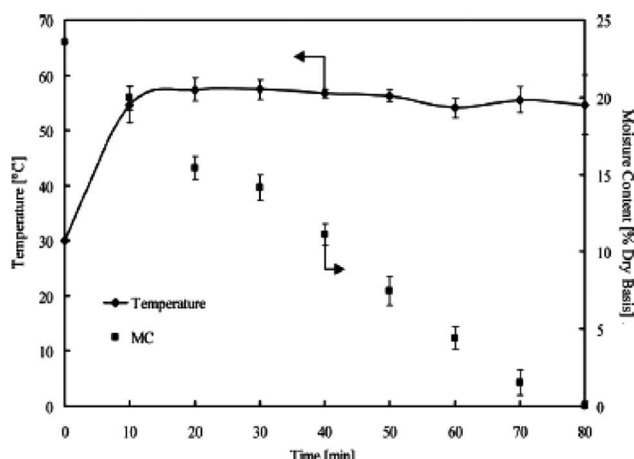


Figure 45. Variations in temperature and moisture over time for drying in the CMCB ($T_1 = 30^\circ\text{C}$; case 2, C-bed). Reprinted from Jindarat et al.^[56] with permission from Taylor & Francis.

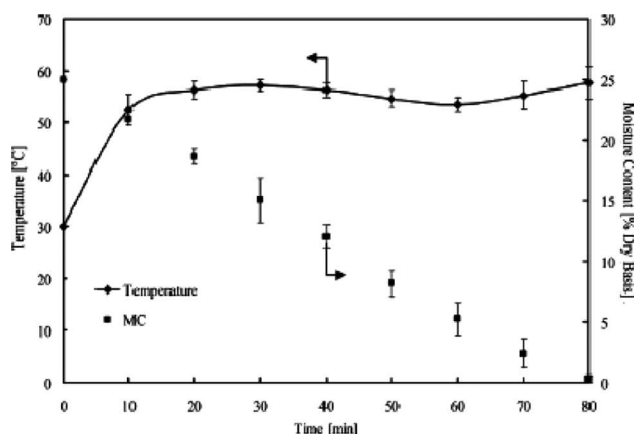


Figure 46. Variations in temperature and moisture over time for drying in the CMCB ($T_1 = 70^\circ\text{C}$, case 3, F-bed). Reprinted from Jindarat et al.^[56] with permission from Taylor & Francis.

(F- or C-bed), and magnetron location on the overall drying kinetics and energy utilization ratio during the drying of a non-hygroscopic porous packed bed, composed of glass beads and water (saturated porous packed bed, $s_0 = 1$) as shown in Fig. 48. The energy analysis can be calculated as discussed above. For exergy analysis, the authors considered the second law of thermodynamics and estimated the total exergy of inflow, outflow, and

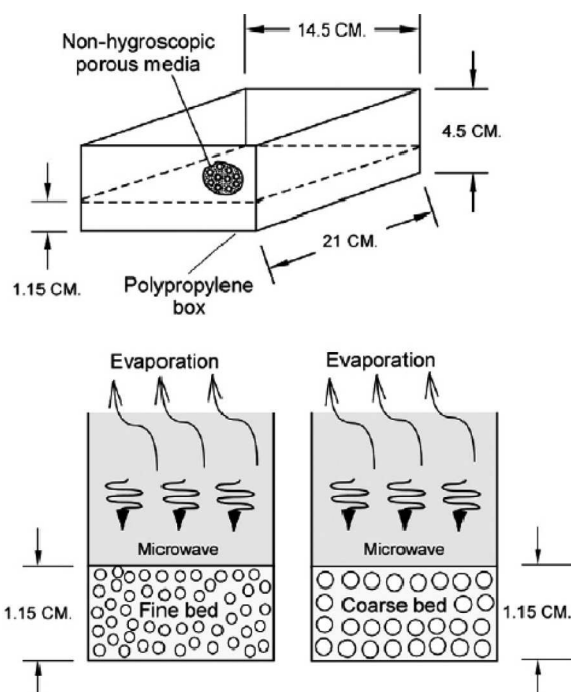


Figure 48. Schematic of drying sample (porous packed bed). Reprinted from *International Communications in Heat and Mass Transfer*, Vol. 39, R. Prommas, P. Rattanadecho, and W. Jindarat, "Energy and exergy analyses in drying process of non-hygroscopic porous packed bed using a combined multi-feed microwave-convective air and continuous belt system (CMCB)," pp. 242–250, 2012, with permission from Elsevier.

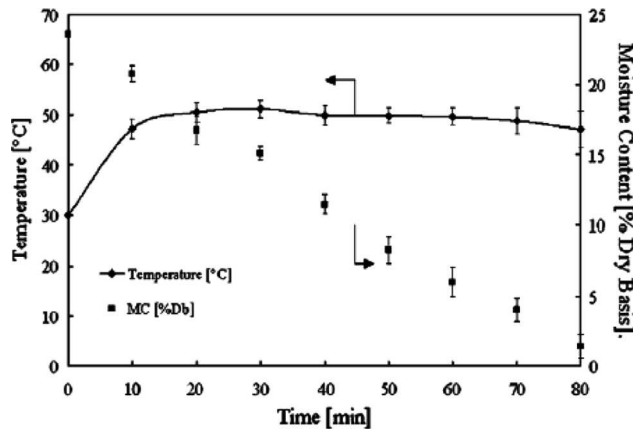


Figure 49. Variations in temperature and moisture over time for drying in the CMCB ($T_1 = 30^\circ\text{C}$, case 1, C-bed). Reprinted from *International Communications in Heat and Mass Transfer*, Vol. 39, R. Prommas, P. Rattanadecho, and W. Jindarat, "Energy and exergy analyses in drying process of non-hygroscopic porous packed bed using a combined multi-feed microwave-convective air and continuous belt system (CMCB)," pp. 242–250, 2012, with permission from Elsevier.

losses of the drying chamber. Exergy of the chamber was analyzed by determining the exergy values at steady-state and the reasons for exergy variations from steady-state. Equation (38) provides the mathematical formulation used to evaluate the exergy balance.^[114] The temperature and moisture variations were determined as a function of time for the C- and F-beds with a constant initial moisture content of 25% (dry basis). In the case of microwave-convective air drying (30°C and 70°C), the moisture profile of the sample continuously decreased at a faster rate compared to the case of convective drying, as shown in Figs. 49 and 50. The energy utilization ratio and exergy efficiency depended on the particle size, hot-air temperature, and magnetron location.

$$\begin{aligned}
 \text{Exergy} = & \underbrace{(u - u_\infty)}_{\text{Internal energy}} - T_\infty \underbrace{(s - s_\infty)}_{\text{Entropy}} \\
 & \underbrace{\frac{P_\infty}{J}(v - v_\infty)}_{\text{Work}} + \underbrace{\frac{V^2}{2gJ}}_{\text{Momentum}} + \underbrace{(z - z_\infty)\frac{g}{g_cJ}}_{\text{Gravity}} \\
 & \sum_c (\mu_c - \mu_\infty)N_c + \underbrace{E_i A_i F_i}_{\text{Radiation}} (3T^4 - T_\infty^4 - 4T_\infty T^4) + \dots \\
 & \text{Chemical}
 \end{aligned}
 \quad (39)$$

where ∞ is the reference condition.

In 2013, Jindarat et al.^[56] analyzed the energy consumption during the drying of biomaterials using a combined unsymmetrical double-feed microwave and vacuum system (CUMV) (Fig. 51). An energy consumption model based on the first law of thermodynamics

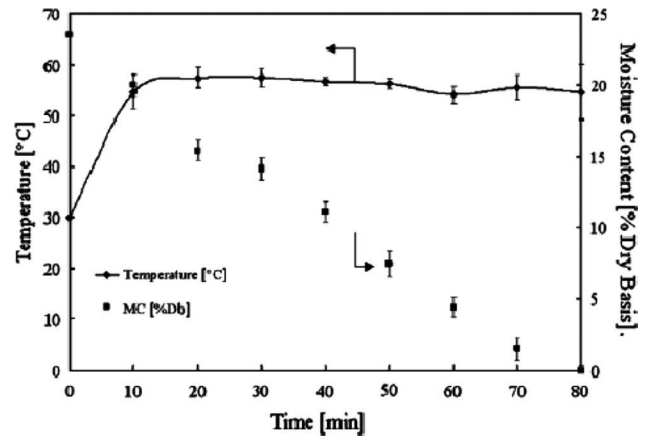


Figure 50. Variations in temperature and moisture over time for drying in the CMCB ($T_1 = 30^\circ\text{C}$, case 2, F-bed). Reprinted from *International Communications in Heat and Mass Transfer*, Vol. 39, R. Prommas, P. Rattanadecho, and W. Jindarat, "Energy and exergy analyses in drying process of non-hygroscopic porous packed bed using a combined multi-feed microwave-convective air and continuous belt system (CMCB)," pp. 242–250, 2012, with permission from Elsevier.

was developed to evaluate energy efficiency. Influences of microwave power, vacuum pressure, and microwave operation mode on energy consumption were considered in detail. To analyze mass transfer in the drying process, they applied the law of conservation of mass for the control volume, as shown in Fig. 52, in which the mass balance equation can be defined as in Eq. (37). Recently, Jindarat et al.^[115] developed an energy model based on the first law of thermodynamics to evaluate



Figure 51. CUMV system. Reprinted from Jindarat et al.^[56] with permission from Taylor & Francis.

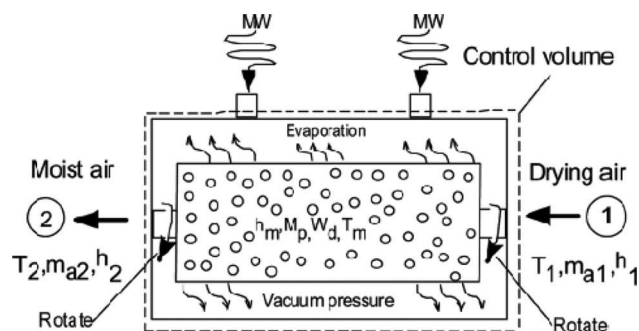


Figure 52. Schematic of the control volume during CUMV drying. Reprinted from Jindarat et al.^[56] with permission from Taylor & Francis.

energy efficiency and specific energy consumption in a combined microwave-hot air spouted bed (CMHS) drying of biomaterial (coffee beans). The influences of hot air temperature and initial weight of coffee beans on energy consumption were considered. For analyzing mass transfer in the drying process, the law of conservation of mass for the control volume is applied, as shown in Fig. 53. The results indicated that the CMHS drying method with the drying conditions of hot air temperature of 60°C, air velocity of 12 m/s, and initial coffee bean weight of 280 g gave a good quality dehydrated coffee bean and involved low specific energy consumption in the drying method. Further, the quality

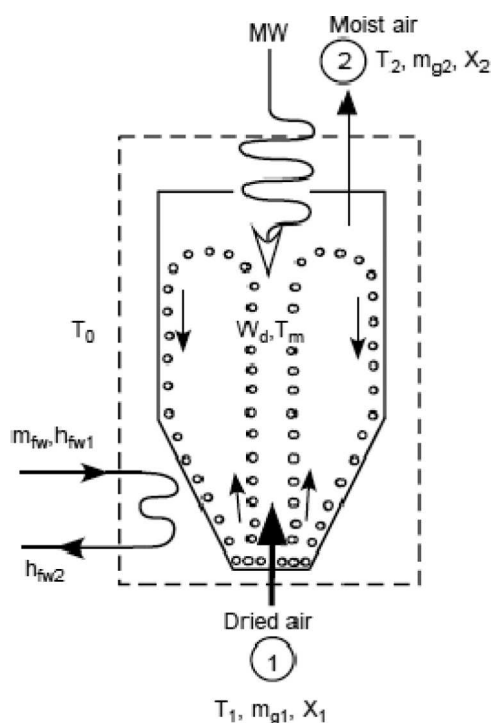


Figure 53. Physical control volume of CMHS drying process using energy analysis. Reprinted from Jindarat et al.^[115] with permission from Taylor & Francis.

of coffee beans dehydrated by the CMHS drying method is found to be superior to the HASB drying method.

Conclusions

Published articles on the kinetic mechanisms of MWD have been reviewed systematically. In particular, the dielectric aspects of the materials to be dried have been examined, including factors affecting methods for measuring and applications of the dielectric properties. From the experimental perspective, the equipment, stability, safety, and regulation of laboratory- and commercial-scale MWD systems have been discussed. Theoretical investigations of thermal and non-thermal equilibrium models, and multiple magnetrons have been described. Finally, future trends in the research and development of MWD are suggested, including the limitations of MWD and the three variables that need to be studied in depth to achieve a full understanding of heat and mass transfer in these systems. This review indicates that MWD alone has several limitations for experimental and commercial-scale applications, such as the non-uniformity of the electromagnetic field within the microwave cavity, the high penetration depth within the dielectric materials, and the fast mass transport of the microwave power (which may alter the quality or texture of food). To overcome these problems, materials to be dried should be in constant motion with a uniformity of power absorbed in the cavity to avoid any hot spots. Combining MWD with conventional or other drying techniques can also be employed. Further research of MWD and/or hybrid drying systems must include an examination of macroscopic equations to simulate the drying process in terms of the heat and mass transfer in porous media. Especially, a MWD associated with a hybrid drying system which consists of multiple-microwave sources has been continuously developing by the authors. For example, hot air is applied at initial stage for 30 min and consecutively hot air is applied associated with microwave energy, or infrared is applied at first stage and MWD is consecutively applied, etc. One-, two-, and three-variable models should include chemical reaction terms. Furthermore, using the three variables considered, the moving-load computational models, in-depth investigations enabling the full explanation of heat and mass transfer properties, and pressure build-up should be possible.^[61]

Nomenclature

a	thermal diffusivity (m^2/s)
\vec{B}	magnetic flux density (Wb/m^2)

C_p	specific heat capacity (J/kgK)
c_p	heat capacity at constant pressure (J/(kg · K))
\bar{D}	electric flux density (C/m)
D_m	effective molecular mass diffusion (m ² /s)
D_p	penetration depth (m)
e	Euler's number (= 2.7182818 ...)
E	electric field intensity (V/m)
f	frequency (Hz)
g_r	gravitational constant (m/s ²)
h_c	heat transfer constant (W/m ² K)
h_m	mass transfer constant (W/m ² K)
\bar{H}	magnetic field intensity (A/m)
H_v	specific heat of vaporization (J/kg)
K	permeability (m ²)
L	material length
\dot{m}	phase change term (kg/m ³ s)
P	microwave power (W)
\vec{P}	energy flux density (W/m ²)
p	pressure (Pa)
q	electric charge density (C/m ³)
Q	microwave power absorbed term (W/m ³)
s	water saturation
S_{11}	reflected scattering coefficient from Port 1
S_{21}	transmitted scattering coefficient from Port 1
S_{22}	reflected scattering coefficient from Port 2
S_{22}	transmitted scattering coefficient from Port 2
T	temperature (°C)
t	time (s)
$\tan \delta$	loss tangent coefficient
V	volume (m ³)

Greek letters

Γ	reflection coefficient
σ	effective conductivity (S/m)
ϵ_0	permittivity of free space (= 8.8514 × 10 ⁻¹²) (F/m)
ϵ_∞	permittivity at the high frequency limit
ϵ_s	static, low-frequency permittivity
ϵ^*	complex (electric) permittivity, $\epsilon' - j\epsilon''$
ϵ_r	relative permittivity
ϵ_r'	relative dielectric constant
ϵ_r''	relative dielectric loss factor
μ^*	complex magnetic permeability, $\mu' - j\mu''$
μ_0	permeability of free space (= 4π × 10 ⁻⁷) (m · kg/s ² · A ²) or (h/m)
μ_r	relative permeability
v	microwave speed in the dielectric material (m/s)
ω	angular frequency, field's frequency (s ⁻¹)
$\tan \delta$	loss tangent coefficient (ϵ''/ϵ')

σ	electric conductivity (1/Ω)
τ	characteristic relaxation time (s)
ρ	density (kg/m ³)
λ_g	wavelength in sample
$\lambda_{free\ space}$	wavelength of free space
λ_{cutoff}	wavelength of cutoff frequency

Subscripts

0	free space
a	air
c	capillary
g	gas
l	liquid water
p	particle
r	relative
v	water vapor
x, z	coordinate axis (m)
∞	ambient condition

Funding

The authors gratefully acknowledge the Thailand Research Fund under the TRF contract Nos. RTA5680007 and TRG5780255, and the National Research Universities Project of the Higher Education Commission for supporting this research.

References

- [1] Metaxas, A.C. Microwave heating. *Journal of Microwave Power and Electromagnetic Energy* **1991**, 5, 237–247.
- [2] Metaxas, A.C.; Meredith, R.J. *Industrial Microwave Heating*; Peter Peregrinus: Herts, UK, 1998.
- [3] Mujumdar, A.S. *Handbook of Industrial Drying*, 4th ed.; CRC Press: Boca Raton, FL, 2014.
- [4] Choi, Y.; Okos, M.R. Thermal properties of liquid foods review. In *Physical and Chemical Properties of Food*, Ed.; Okos, M.R. American Society of Agricultural Engineers: St. Joseph, MI, 1986; 5–77.
- [5] Chang, K.; Ruan, R.R.; Chen, P.L. Simultaneous heat and moisture transfer in cheddar cheese during cooling. I. Numerical simulation. *Drying Technology* **1998**, 16(7), 1447–1458.
- [6] Kaensup, W.; Wongwises, S.; Chutima, S. Drying of pepper seeds using a combined microwave fluidized bed dryer. *Drying Technology* **1998**, 16(3–5), 853–862.
- [7] Kaensup, W.; Wongwises, S. Combined microwave/fluidized bed drying of fresh pepper corns. *Drying Technology* **2004**, 22(4), 779–794.
- [8] Fakhouri, O.M.; Ramaswamy, S.H. Temperature uniformity of microwave heated foods as influenced by product type and composition. *Food Research International* **1993**, 26(2), 89–95.
- [9] Alibas, I. Microwave, vacuum, and air drying characteristics of collard leaves. *Drying Technology* **2009**, 27, 1266–1273.
- [10] Basak, T.; Meenakshi, A. A theoretical analysis on microwave heating of food slabs attached with ceramic

- plates: Role of distributed microwave incidence. *Food Research International* **2006**, 39(8), 932–944.
- [11] Regier, M.; Schubert, H. Microwave processing. In *The Microwave Processing of Foods*; Schubert, H.; Regier, M. Eds.; Woodhead Publishing, Sawston, Cambridge, UK, 2001.
 - [12] Afrin, N.; Zhang, Y.; Chen, J.K. Thermal lagging in living biological tissue based on non-equilibrium heat transfer between tissue, arterial and venous bloods. *International Journal of Heat and Mass Transfer* **2011**, 54, 2419–2426.
 - [13] Perre, P.; Turner, I.W. Microwave drying of softwood in an oversized waveguide: Theory and experiment. *AIChE Journal* **1997**, 43(10), 2579–2595.
 - [14] Vongpradubchai, S.; Rattanadecho, P. Microwave and hot air drying of wood using a rectangular waveguide. *Drying Technology* **2011**, 29(4), 451–460.
 - [15] Basak, T.; Meenakshi, A. Influence of ceramic supports on microwave heating for composite dielectric food slabs. *AIChE Journal* **2006**, 52(6), 1995–2007.
 - [16] Basak, T.; Rao, B.S. Role of ceramic composites and microwave pulsing on efficient microwave processing of pork meat samples. *Food Research International* **2011**, 44, 2679–2697.
 - [17] Basak, T. Role of resonance on microwave heating of oil–water emulsions. *AIChE Journal* **2004**, 50, 2659–2675.
 - [18] Ratanadecho, P. Microwave heating using a rectangular wave guide. Ph.D. thesis, Nakaoka University of Technology, Japan, 2002.
 - [19] Basak, T.; Samanta, S.K.; Jindamwar, A. A novel concept on discrete samples for efficient microwave processing of materials. *Chemical Engineering Science* **2008**, 63(12), 3292–3308.
 - [20] Tsotsas, E.; Mujumdar, A.S. *Modern Drying Technology*, Vol. 5; VCH Wiley: Weinheim: Germany, 2014.
 - [21] Llave, Y.; Terada, Y.; Fukuoka, M.; Sakai, N. Dielectric properties of frozen tuna and analysis of defrosting using a radio-frequency system at low frequencies. *Journal of Food Engineering* **2014**, 139, 1–9.
 - [22] Tulasidas, T.N.; Raghavan, G.S.V.; Mujumdar, A.S. Microwave drying of grapes in a single mode cavity at 2450 MHz-I: drying kinetics; and II: quality and energy aspects. *Drying Technology* **1995**, 13(8–9), 1949–1992.
 - [23] Dev, S.R.S.; Gariépy, Y.; Raghavan, G.S.V. Measurement of dielectric properties and finite element simulation of microwave pretreatment for convective drying of grapes. *Progress in Electromagnetic Research Online* **2009**, 5(7), 690–695.
 - [24] Okiror, G.P.; Jones, C.L. Effect of temperature on the dielectric properties of low acyl gellan gel. *Journal of Food Engineering* **2012**, 113, 151–155.
 - [25] Tanaka, F.; Uchino, T.; Hamanaka, D.; Atungulu, G.G.; Hung, Y.-C. Dielectric properties of mirin in the microwave frequency range. *Journal of Food Engineering* **2008**, 89, 435–440.
 - [26] Guo, W.; Liua, Y.; Zhua, X.; Wanga, S. Dielectric properties of honey adulterated with sucrose syrup. *Journal of Food Engineering* **2011**, 107, 1–7.
 - [27] Feng, H.; Tang, J.; Cavalieri, R.P. Dielectric properties of dehydrated apples as affected by moisture and temperature. *Transactions of the American Society of Agricultural Engineers* **2002**, 45(1), 129–135.
 - [28] Sipahioglu, O.; Barringer, S.A. Dielectric properties of vegetables and fruits as a function of temperature, ash, and moisture content. *Journal of Food Science* **2003**, 68(1), 234–239.
 - [29] Solyom, K.; Kraus, S.; Mato, R.B.; Gaukel, V.; Schuchmann, H.P.; José Cocero, M. Dielectric properties of grape marc: Effect of temperature, moisture content and sample preparation method. *Journal of Food Engineering* **2013**, 119, 33–39.
 - [30] Tang, J.; Feng, H.; Lau, M. Microwave heating in food processing. In Young, X.; Tang, J. eds.; *Advances in Agricultural Engineering*; World Scientific Publishing Co.: Singapore, 2002; 1–43.
 - [31] Roebuck, B.D.; Goldblith, S.A. Dielectric properties of carbohydrate–water mixtures at microwave frequencies. *Journal of Food Science* **1972**, 37(1), 199–204.
 - [32] Wang, R.; Zhang, M.; Mujumdar, A.S.; Jiang, H. Effect of salt and sucrose content on dielectric properties and microwave freeze drying behavior of re-structured potato slices. *Journal of Food Engineering* **2011**, 106, 290–297.
 - [33] Wang, Y.; Zhang, M.; Mujumdar, A.S.; Joseph, M.K.; Azam, S.M.R. Effect of blanching on microwave freeze drying of stem lettuce cubes in a circular conduit drying chamber. *Journal of Food Engineering* **2012**, 113, 177–185.
 - [34] Kristiawan, M.; Sobolik, V.; Klíma, L.; Allaf, K. Effect of expansion by instantaneous controlled pressure drop on dielectric properties of fruits and vegetables. *Journal of Food Engineering* **2011**, 102, 361–368.
 - [35] Venkatesh, M.S.; Raghevan, G.S.V. An overview of dielectric properties measuring techniques. *Canadian Biosystems Engineering* **2005**, 47, 15–29.
 - [36] Tereshchenko, O.V.; Buesink, F.J.K.; Leferink, F.B.J. An overview of the techniques for measuring the dielectric properties of materials. In *General Assembly and Scientific Symposium, 2011 XXXth URS*, Istanbul, August 13–20; IEEE: Piscataway, NJ, 2011.I.
 - [37] Hewlett Packard Corporation. Dielectric Probe Kit 85070A. Palo Alto, CA: Research and Development Unit, Test and Measurements Laboratories, Hewlett Packard Corporation, 1992.
 - [38] Ratanadecho, P. The simulation of microwave heating of wood using a rectangular wave guide: Influence of frequency and sample size. *Chemical Engineering Science* **2006**, 61, 4798–4811.
 - [39] Cronin, N.J. *Microwave and Optical Waveguides*; Taylor & Francis: London, 1995.
 - [40] Ratanadecho, P.; Aoki, K.; Akahori, M. Experimental and numerical study of microwave drying in unsaturated porous material. *International Journal of Heat and Mass Transfer* **2001**, 28, 605–616.
 - [41] Ratanadecho, P.; Aoki, K.; Akahori, M. A numerical and experimental investigation of the modeling of microwave drying using a rectangular wave guide. *Drying Technology* **2001**, 19(9), 2209–2234.
 - [42] Ratanadecho, P.; Aoki, K.; Akahori, M. Experimental and numerical study of microwave drying in unsaturated porous material. *International Communications in Heat and Mass Transfer* **2001**, 28(5), 605–616.

- [43] Jindarat, W.; Rattanadecho, R.; Vongpradubchaia, S.; Pianroj, Y.Y. Analysis of energy consumption in drying process of non-hygroscopic porous packed bed using a combined multi-feed microwave-convective air and continuous belt system (CMCB). *Drying Technology* **2011**, 29(8), 926–938.
- [44] Prommas, R.; Rattanadecho, P.; Jindarat, W. Energy and exergy analyses in drying process of non-hygroscopic porous packed bed using a combined multi-feed microwave-convective air and continuous belt system (CMCB). *International Communications in Heat and Mass Transfer* **2012**, 39, 242–250.
- [45] Cohen, J.S.; Yang, T.C.S. Progress in food dehydration. *Trends in Food Science & Technology* **1995**, 6(1), 20–25.
- [46] Zhang, M.; Tang, J.; Mujumdar, A.S.; Wang, S. Trends in microwave-related drying of fruits and vegetables. *Trends in Food Science & Technology* **2006**, 17, 524–534.
- [47] Feng, H.; Tang, J. Microwave finish drying of diced apples in a spouted bed. *Journal of Food Science* **1998**, 63(4), 679–683.
- [48] Huang, L.; Zhang, M.; Mujumdar, A.S.; Lim R.-X. Comparison of four drying methods for re-structured mixed potato with apple chips. *Journal of Food Engineering* **2011**, 103, 279–284.
- [49] Jiang, H.; Zhang, M.; Liu Y.; Mujumdar, A.S.; Liu, H. The energy consumption and color analysis of freeze/microwave freeze banana chips. *Food and Bioprocess Technology* **2013**, 91, 464–472.
- [50] Markowski, M.; Bondaruk, J.; Błaszczyk, W. Rehydration behavior of vacuum-microwave dried potato cubes. *Drying Technology* **2009**, 27(2), 296–305.
- [51] Wang, Y.; Zhang, M.; Mujumdar, A.S. Effect of cassava starch gel, fish gel and mixed gels and thermal treatment on structure development and various quality parameters in microwave vacuum-dried gel slices. *Food Hydrocolloids* **2013**, 33, 26–37.
- [52] Zhang, F.; Zhang, M.; Mujumdar, A.S. Drying characteristics and quality of restructured wild cabbage chips processed using different drying methods. *Drying Technology* **2011**, 29(6), 682–688.
- [53] Thussu, S.; Datta, A. Fundamentals-based quality prediction: Texture development during drying and related processes. *Procedia Food Science* **2011**, 1, 1209–1215.
- [54] Namsanguan, Y.; Tia, W.; Devahastin, S.; Soponronnarit, S. Drying kinetics and quality of shrimp undergoing different two-stage drying processes. *Drying Technology* **2004**, 22(4), 759–778.
- [55] Charoenvai, S.; Yingyuen, W.; Jewyee, A.; Rattanadecho, P.; Vongpradubchai, S. Comparative evaluation on product properties and energy consumption of single microwave dryer and combination of microwave and hot air dryer for durian peel particleboards. *Energy Procedia* **2013**, 34, 479–492.
- [56] Jindarat, W.; Sungsoontorn, S.; Rattanadecho, P. Analysis of energy consumption in drying process of biomaterials using a combined unsymmetrical double-feed microwave and vacuum system (CUMV) —Case study: Tea leaves. *Drying Technology* **2013**, 31 (10), 1138–1147.
- [57] Yang, H. C.; Püschner, P. Heat transfer with the speed of light using microwaves in industrial chemical processes. Presented at AchemAsia 2013, Beijing, China, May 13–16, 2013.
- [58] Micro Denshi Co., Ltd. <http://www.microdenshi.co.jp/en/products/>.
- [59] Occupational Health and Safety Administration (OSHA). Radiofrequency and microwave radiation. 2009. <http://www.osha.gov/SLTC/radiofrequencyradiation/>.
- [60] International Radiation Protection Association (IRPA). International Commission on Non-Ionizing Radiation Protection (ICNIRP) Guidelines: For limiting exposure to time-varying electric, magnetic and electromagnetic fields (up to 300 GHz). *Health Physics* **1988**, 54, 492–522.
- [61] Institute of Electrical and Electronics Engineers (IEEE). Technical information statement on: Human exposure to microwaves and other radio frequency electromagnetic fields. *IEEE Engineering in Medicine and Biology Magazine* **1995**, 14, 336–337.
- [62] Institute of Electrical and Electronics Engineers (IEEE). Standard for safety levels with respect to human exposure to radio frequency electromagnetic fields 3 kHz to 300 GHz. IEEE/ANSI, C95.1., 2005.
- [63] National Radiological Protection Board (NRPB) and the Health Protection Agency. *Review of the Scientific Evidence for Limiting Exposure to Electromagnetic Fields (0–300 GHz)*; 2004.
- [64] Fujiwara, O.; Kato, A. Computation of SAR inside eyeball for 1.5-GHz microwave exposure using finite-difference time domain technique. *IEICE Transaction* **1994**, E77-B, 732–737.
- [65] Karampatzakis, A.; Samaras, T. Numerical modeling of heat transfer and fluid flow transfer in the human eye under millimeter wave exposure. *Bioelectromagnetics* **2013**, 34, 291–299.
- [66] International Commission on Non-Ionizing Radiation Protection (ICNIRP). Guidelines for limiting exposure to time-varying electric, magnetic and electromagnetic fields (up to 300 GHz). *Health Physics* **1998**, 74, 494–522.
- [67] IEEE. IEEE Standard for Safety Levels with Respect to Human Exposure to Radio Frequency Electromagnetic Fields, 3 kHz to 300 GHz. IEEE Standard C95 1999, 1.
- [68] Taflove, A.; Brodwin, M.E. Computation of the electromagnetic fields and induced temperature within a model of the microwave-irradiated human eye. *IEEE Transactions on Microwave Theory and Techniques* **1975**, 23(11), 888–896.
- [69] Lagendijk, J.J.W. A mathematical model to calculate temperature distribution in human and rabbit eye during hyperthermic treatment. *Physics in Medicine and Biology* **1982**, 27, 1301–1311.
- [70] Scott, J. A finite element model of heat transport in the human eye. *Physics in Medicine and Biology* **1988**, 33, 227–241.
- [71] Scott, J. The computation of temperature rises in the human eye induced by infrared radiation. *Physics in Medicine and Biology* **1988**, 33, 243–257.
- [72] Kumar, S.; Acharya, S.; Beuerman, R.; Palkama, A. Numerical solution of ocular fluid dynamics in a rabbit eye: Parametric effects. *Annals of Biomedical Engineering* **2006**, 34, 530–544.

- [73] Ooi, E.; Ng, E.Y.K. Simulation of aqueous humor hydrodynamics in human eye heat transfer. *Computers in Biology and Medicine* **2008**, *38*, 252–262.
- [74] Ooi, E.H.; Ng, E.Y.K. Effects of natural convection inside the anterior chamber. *International Journal for Numerical Methods in Biomedical Engineering* **2011**, *27*, 408–423.
- [75] Pennes, H.H. Analysis of tissue and arterial blood temperatures in the resting human forearm. *Journal of Applied Physiology* **1948**, *1*, 93–122.
- [76] Flyckt, V.M.M.; Raaymakers, B.W.; Lagendijk, J.J.W. Modeling the impact of blood flow on the temperature distribution in the human eye and the orbit: Fixed heat transfer coefficients versus the Pennes bioheat model versus discrete blood vessels. *Physics in Medicine and Biology* **2006**, *51*, 5007–5021.
- [77] Ng, E.Y.K.; Ooi, E.H. FEM simulation of the eye structure with bioheat analysis. *Computer Methods and Programs in Biomedicine* **2006**, *82*, 268–276.
- [78] Ooi, E.H.; Ng, E.Y.K. Ocular temperature distribution: a mathematical perspective. *Journal of Mechanics in Medicine and Biology* **2009**, *9*, 199–227.
- [79] Wessapan, T.; Srisawatdhisukul, S.; Rattanadecho, P. The effects of dielectric shield on specific absorption rate and heat transfer in the human body exposed to leakage microwave energy. *International Communications in Heat and Mass Transfer* **2011**, *38*, 255–262.
- [80] Wessapan, T.; Rattanadecho, P. Specific absorption rate and temperature increase in the human eye due to electromagnetic fields exposure at different frequencies. *International Journal of Heat and Mass Transfer* **2013**, *64*, 426–435.
- [81] Wessapan, T.; Rattanadecho, P. Influence of ambient temperature on heat transfer in the human eye during exposure to electromagnetic fields at 900 MHz. *International Journal of Heat and Mass Transfer* **2014**, *70*, 378–388.
- [82] Ayappa, K.G.; Davis, H.T.; Davis, E.A.; Gordon, J. Analysis of microwave heating of materials with temperature dependent properties. *AIChE Journal* **1991**, *37*(3), 313–322.
- [83] Whitaker, S. A theory of drying in porous media. *Advanced Heat Transfer* **1977**, *13*, 119–203.
- [84] Bories, S.A. Fundamental of drying of capillary-porous bodies. In *Convective Heat and Mass Transfer in Porous Media*; Kakac, S.; Kilis, B.; Kulacki, F.; Arinc, F. Eds.; NATO ASI series, Vol. 196; Kluwer Publishers: Dordrecht, the Netherlands, 1991; 39–434.
- [85] Boukadida, N.; Ben Nasrallah, S. Two dimensional heat and mass transfer during convective drying of porous media. *Drying Technology* **1995**, *13*(3), 661–694.
- [86] Ni, H.; Datta, A.K.; Torrance, K.E. Moisture transport in intensive microwave heating of biomaterials: A multiphase porous media model. *International Journal of Heat and Mass Transfer* **1999**, *42*, 1501–1512.
- [87] Feng, H.; Tang, J.; Cavalieri, R.P.; Plumb, O.A. Heat and mass transport in microwave drying of porous materials in a spouted bed. *AIChE Journal* **2001**, *7*, 1499–1512.
- [88] Rattanadecho, P.; Pakdee, W.; Stakulcharoen, J. Analysis of multiphase flow and heat transfer: Pressure buildup in an unsaturated porous slab exposed to hot gas. *Drying Technology* **2008**, *26*, 39–53.
- [89] Knoerzer, K.; Regier, M.; Hardy, E.H.; Schubert, H.; Schuchmann, H.P. Simultaneous microwave heating and three-dimensional MRI temperature mapping. *Innovative Food Science & Emerging Technologies* **2009**, *10*, 537–544.
- [90] Chen, G.; Wang, W.; Mujumdar, A.S. Theoretical study of microwave heating patterns on batch fluidized bed drying of porous material. *Chemical Engineering Science* **2001**, *56*, 6823–6835.
- [91] Bhattacharya, M.; Basak, T. On the analysis of microwave power and heating characteristics for food processing: Asymptotes and resonances. *Food Research International* **2006**, *39*, 1046–1057.
- [92] Suwannapum, N.; Rattanadecho, P. Analysis of heat-mass transport and pressure buildup induced inside unsaturated porous media subjected to microwave energy using a single (TE₁₀) mode cavity. *Drying Technology* **2011**, *29*, 1010–1024.
- [93] Sungsoontorn, S.; Rattanadecho, P.; Pakdee, W. One-dimensional model of heat and mass transports and pressure built up in unsaturated porous materials subjected to microwave energy. *Drying Technology* **2011**, *29*(2), 189–204.
- [94] Ayappa, K.G. Modeling transport processes during microwave heating: a review. *Reviews in Chemical Engineering* **1997**, *13*(2), 1–68.
- [95] Fu, W.; Metaxas, A.C. A mathematical derivation of power penetration depth for thin lossy materials. *Journal of Microwave Power and Electromagnetic Energy* **1992**, *27*(4), 217–222.
- [96] Ni, H.; Datta, A.K. Heat and moisture transfer in baking of potato slabs. *Drying Technology* **1999**, *17*(10), 2069–2092.
- [97] Rakesh, V.; Datta, A.K. Microwave puffing: Determination of optimal conditions using a coupled multiphase porous media—large deformation model. *Journal of Food Engineering* **2011**, *107*, 152–163.
- [98] Chua, K.J.; Chou, S.K.; Ho, J.C. A comparative study of time-varying thermal and non-thermal drying methods for bioproducts. *Applied Biotechnology Food Science and Policy* **2003**, *1*, 115–123.
- [99] Zhang, D.; Mujumdar, A.S. Deformation and stress-analysis of porous capillary bodies during intermittent volumetric thermal drying. *Drying Technology* **1992**, *10*(2), 421–443.
- [100] Gong, Z.X.; Mujumdar, A.S.; Itaya, Y.; Mori, S.; Hasatani, M. Microwave drying of clay and non-clay media: Heat and mass transfer and quality aspects. *Drying Technology* **1998**, *16*(6), 1119–1152.
- [101] Itaya, Y.; Kobayashi, T.; Hayakawa, K. Three-dimensional heat and mass transfer with viscoelastic strain-stress formation in composite food during drying. *International Journal of Heat and Mass Transfer* **1995**, *38*(7), 1173–1185.
- [102] Gunasekaran, S. Pulsed microwave-vacuum drying of food materials. *Drying Technology* **1999**, *17*(3), 395–412.
- [103] Raghavan, G.S.V.; Silveira, A.M. Shrinkage characteristics of strawberries osmotically dehydrated in combination with microwave drying. Presented at ADC'99, Bali, Indonesia, 1999.

- [104] Raghavan, G.S.V.; Venkatachalapathy, K. Shrinkage of strawberries during microwave drying. *Drying Technology* **1999**, 17(10), 2309–2321.
- [105] Sanga, E.; Mujumdar, A.S.; Raghavan, G.S.V. Principles and applications of microwave drying. In *Drying Technology in Agriculture and Food Sciences*; Mujumdar, A.S. Ed. Oxford IBH: Delhi, India, 2001. Published simultaneously by Science Publishers: Enfield, NH, 2001; 253–289.
- [106] Basak, T. Role of lateral and radial irradiations on efficient microwave processing of food cylinders. *Chemical Engineering Science* **2007**, 62, 3185–3196.
- [107] Chaiyo, K.; Rattanadecho, P. Numerical analysis of heat-mass transport and pressure buildup of unsaturated porous medium in a rectangular waveguide subjected to a combined microwave and vacuum system. *International Journal of Heat and Mass Transfer* **2013**, 65, 826–844.
- [108] Perré, P.; May, B.K. A numerical drying model that accounts for the coupling between transfers and solid mechanics: Case of highly deformable products. *Drying Technology* **2001**, 19(8), 1629–1643.
- [109] Perré, P.; Turner, I.W. A 3-D version of TransPore: A comprehensive heat and mass transfer computational model for simulating the drying of porous media. *International Journal of Heat and Mass Transfer* **1999**, 42(24), 4501–4521.
- [110] Rattanadecho, P.; Klinbun, W. Numerical analysis of natural convection in porous media subjected to electromagnetic energy using local thermal non-equilibrium (LTNE) models. *Drying Technology* **2012**, 30(16), 1896–1905.
- [111] Klinbun, W.; Rattanadecho, P. Numerical model of microwave driven convection in multilayer porous packed bed using a rectangular waveguide. *Journal of Heat Transfer* **2012**, 134, 042605–1–042605–10.
- [112] Keangin, P.; Rattanadecho, P. Analysis of heat transport on local thermal non-equilibrium in porous liver during microwave ablation. *International Journal of Heat and Mass Transfer* **2013**, 67, 46–60.
- [113] Akpınar, E.K.; Midilli, A.; Bicer, Y. The first and second law analyses of thermodynamic of pumpkin drying process. *Journal of Food Engineering* **2006**, 72, 320–331.
- [114] Ahern, J.E. *The Exergy Method of Energy Systems Analysis*; John Wiley: New York, 1980.
- [115] Jindarat, W.; Sungsoontorn, S.; Rattanadecho, P. Analysis of energy consumption in a combined microwave-hot air spouted bed (CMHS) drying of biomaterial: Coffee beans. *Experimental Heat Transfer* **2015**, 28(2), 107–124.